Chidlow, S, Chong, W and Teodorescu, M

On the two-dimensional solution of both adhesive and non-adhesive contact problems involving functionally graded materials

European Journal of Mechanics - A/Solids, 2013, 39 (May-June). pp. 86-103.
10.1016/j.euromechsol.2012.10.008

On the two-dimensional solution of both adhesive and non-adhesive contact problems involving functionally graded materials

S. J. Chidlow[a], W. W. F. Chong[b], M. Teodorescu[a,c1]

[a]*School of Engineering, Cranfield University, Cranfield, MK43 0AL, UK*
[b]*Wolfson School of Mechanical and Manufacturing Engineering, Loughborough University, Loughborough, LE11 3TU, UK*
[c]*Baskin School of Engineering, University of California at Santa Cruz, CA USA*

Abstract

This paper presents a semi-analytical algorithm for the determination of the contact half width and surface pressure which results from both adhesive and non-adhesive contact problems involving functionally graded materials (FGM). The inhomogeneously elastic solid comprises a graded elastic coating whose shear modulus depends exponentially on the vertical coordinate and a homogeneously elastic substrate. The solid is assumed to be in a state of plane strain and thus a two-dimensional analysis is performed within this work.

Using the work of Chidlow et al. (2011a) as a starting point, we derive a pair of integral equations which may be used to determine approximations to the contact pressure when either the surface deflection or the deflection gradient is known over the contact region. As these integral equations are non-singular, we use Galerkin's method to approximate the contact pressure and it is found that relatively small trial spaces allow accurate computation of the pressure. Information about the prescribed load is then used to formulate an iterative algorithm to determine the contact half width.

[1]*Corresponding author's email address : mteodorescu@soe.ucsc.edu*

A selection of numerical results are presented using this method and it is found that the solutions computed here compare favourably with those of other authors. A further investigation is then conducted into the solution of adhesive contact problems using the assumptions of Maugis (1992) and Johnson and Greenwood (2008) to inform the nature of the adhesive stresses outside of the contact. It is found that both JKR-like and DMT-like behaviour can be observed in contact problems involving FGMs.

1. Introduction

Functionally graded materials are inhomogeneous and consequently their properties (e.g mechanical, chemical) continuously change throughout their volume. As these materials can be designed to possess certain characteristics, they are ideally suited for use as protective coatings. However, a good choice of coating requires knowledge of the underlying properties of the substrate and the physical context of the application. This information is usually obtained from a combination of both theoretical studies and experimental data and thus the ability to model such problems mathematically is crucial.

The classical problem of contact between a homogeneously elastic solid and a rigid body was first solved by Hertz (1881) who provided analytical expressions for the pressures that result from contact between a homogeneously elastic medium and a cylinder (two-dimensional) or a ball (three-dimensional). Additionally, he advanced analytical equations from which the contact radius can be determined provided that the applied load is known in both cases. These results are still used today and provide perhaps the only closed form solutions of the contact problem. However, as these results are valid only for a homogeneous solid, they cannot be used to model FGMs.

A further limitation of the Hertzian model is that it does not allow for adhesion in the contact between two bodies and predicts no contact between bodies under zero load. It has been observed however that bodies with clean, dry surfaces exhibit strong adhesion and in fact give rise to a finite non-zero contact area even under zero load. The inability of Hertzian theory to accurately model such problems has resulted in researchers trying to find new models to describe adhesive contacts. Possibly the most well known models in a three-dimensional context were proposed by Johnson et al. (1971) and Derjaguin et al. (1975). Johnson et al. (1971) proposed that adhesion occurs only within the contact and that infinitely large tensile stresses are experienced at the edges of the contact whilst Derjaguin et al. (1975) hypothesised that adhesion occurs only outside of the contact whilst the contact profile is given using Hertzian theory. It has been found that the JKR model corresponds well to soft materials with large surface energy and radius whilst the DMT model corresponds well to hard materials of small radius and low surface energy. Maugis (1992) then proposed a Dugdale model to characterise the adhesion between solids which allowed the contact radius and total load to be characterised as a function of a single variable λ. As λ increases from zero to infinity there is a smooth transition between the DMT and JKR models. The only drawback in this model is the difficulty in relating the contact radius and load directly to each other using a single equation. This was remedied by Carpick et al. (1999) who presented a simple general equation that approximates Maugis's solution closely.

The work conducted on adhesive contacts in three-dimensional solids was generalised by Johnson and Greenwood (2008) to the two-dimensional line case. The authors used the assumptions of Maugis (1992) to determine the adhesive forces outside of the contact whilst the adhesive force

within the contact was determined using a Westergaard stress function. The contact pressure was assumed to be given by Hertzian theory. Using a non-dimensional parameter λ similar to the so-called 'Tabor' parameter introduced by Fuller and Tabor (1975), it was found that as λ increases from zero to infinity, the contact model transitions smoothly between the two-dimensional DMT and JKR models as was found in the three-dimensional case. This problem was also investigated by Wu (2009) who used a Lennard Jones potential to determine numerical solutions to the contact problem and found that his results compared well with Johnson and Greenwood for larger values of the Tabor parameter but in the rigid body limit corresponding to $\lambda \rightarrow 0$ his results behaved like the two-dimensional Bradley (1932) model rather than the DMT model.

In addition to investigations on the adhesive nature of contacts that involve homogeneous materials, there has been some investigation into the adhesive behaviour of layered solids. This is primarily because there are many applications (e.g biological tissues and soft bearing surfaces in artificial joint replacements) where thin compliant layers are strongly affected by adhesion in contact. Mary et al. (2006) presented a semi-analytical model that describes adhesive contact between a layered solid and an axisymmetric indenter. The accuracy of this model was validated experimentally and by comparison with numerical results produced using the finite element method (FEM). Johnson and Sridhar (2000) derived a JKR-like model to describe adhesive contacts between a solid comprising a homogeneously elastic coating bonded to a substrate and a rigid indenter. A selection of numerical results for a variety of different coatings were presented and the authors found that the JKR model using the elastic properties of the coating agreed well with their numerical results when the coating is thick whilst the JKR model using the elastic layers of the substrate agreed well

with their obtained results when the coating was thin. McGuiggan et al. (2007) compared experimental results obtained for the surface force apparatus (SFA) which comprises three distinct layers with numerical results obtained using FEM. The authors concluded that the obtained pull-off force for a layered solid can vary significantly from that predicted by the JKR model for a homogeneous material.

The majority of models propounded to solve contact problems involving inhomogeneously elastic materials however consider only non-adhesive contact. Early attempts at modelling inhomogeneous materials comprising a distinct coating and substrate assume that the coating is homogeneously elastic whilst the substrate is rigid (e.g Hannah (1951)). If the additional assumption is made that the homogeneous layer is very thin, analytical solutions for the contact pressure may be derived (e.g Barber (1990)). We note however that this situation is far from realistic and thus these models are severely limited in their application.

A popular idea which has been used with great success is to assume that the modulus of elasticity within the FGM is isotropic in the horizontal directions and depends only on the vertical coordinate in some pre-determined way. The most commonly used choices assume that the modulus of elasticity follows either a simple power law or an exponential variation. Giannakopoulos and Suresh (1997) used both the power law and exponential approximations to derive analytical solutions for the stresses and displacements induced within a three-dimensional body by the application of a point force to the solid surface. These results were then compared to numerical solutions computed using the finite element method (FE) and showed good agreement.

A technique that can be used to reduce the complexity of the full contact problem is to as-

sume that the solid is in a state of plane strain. This allows the removal of one of the horizontal variables from the problem and thus a simpler two-dimensional analysis may be performed. This approach was used by Guler and Erdogan (2004) and separately by Ke and Wang (2006), Ke and Wang (2007) who solved the two-dimensional contact problem using Fourier transform methods. Utilising solutions that result from the application of point forces to the solid surface, these authors formulated singular integral equations for the stamp problem which were solved using numerical quadrature. Both sets of authors produce results which agree well with each other. An alternate approach used by Chidlow et al. (2011a), Chidlow et al. (2011b) formulates the sub-surface stresses, displacements and contact pressure in terms of Fourier series. The underlying assumption used in the derivation of these models is that as the induced stresses die very quickly away from the contact area, the contact problem need only be solved in a small section of the solid rather than the solid as a whole. The resulting models are theoretically analytic if the contact pressure is known exactly but due to the infinite summations that arise some small degree of error will be incurred from the truncation of these series. This approach was also used by Teodorescu et al. (2009) who presented an iterative algorithm from which the contact pressure and contact radius resulting from contact by a rigid cylinder may be determined. However these authors model the coating and substrate as distinct yet homogeneous layers whilst Chidlow et al. (2011a) model the coating using the exponential variation assumption.

The work contained within this paper considers both non-adhesive and Maugis-type adhesive contacts that occur between a rigid punch and an inhomogeneously elastic solid comprising an FGM coating-substrate. Using the work of Chidlow et al. (2011a) as a starting point, we derive

an iterative algorithm (given by (46) and outlined in figure (4) for non-adhesive contacts, (74), (77) and outlined in figure (10) for adhesive contacts) that allows the determination of the contact footprint when both the surface deflection or its gradient and the total load are known. The proposed algorithm is very simple in form as it requires only the computation of the coefficients in the Fourier series expansion of the applied pressure which are calculated from a simple explicit formula.

The layout of this paper is as follows. In section 2 we introduce the governing equations of the contact problem and highlight the key results of Chidlow et al. (2011a). In section 3 we formulate the integral equations that relate the pressure and surface deflection and derive an explicit formula from which the coefficients in the Fourier series expansion of the pressure and thus the pressure itself may be computed. In section 4, we present a selection of numerical results that validate the accuracy of this solution technique. An iterative algorithm capable of approximating both the contact half-width and contact pressure is introduced in section 5 and some results are presented using this method. Finally, we conduct an investigation into the solution of adhesive contact problems in section 6 and summarise our work and its implications in section 7.

2. FGM Modelling

2.1. Inhomogeneously elastic layered solid

Consider an inhomogeneously elastic solid in a state of plane strain occupying $-L \leq x \leq L, -\infty < y \leq 0$. The solid is split into two distinct regions which represent a functionally graded coating of thickness h and a homogeneously elastic substrate of infinite extent. The shear modulus within the

solid is defined as

$$\mu(y) = \begin{cases} \mu_1 e^{\alpha y}, & -h \leq y \leq 0, \\ \mu_0, & -\infty < y < -h \end{cases} \tag{1}$$

so that the inhomogeneity of the coating is approximated using a simple exponential function. We note that if $\mu_1/\mu_0 > 1$ then the coating is harder than the substrate whilst if $\mu_1/\mu_0 < 1$ the coating is softer than the substrate. The Poisson ratio of both the coating and substrate are assumed to be constant and equivalent and thus $\nu^{(c)} = \nu^{(s)} = \nu$. Please note as Hooke's laws do not apply for the incompressible case $\nu = 0.5$, we apply the constraint $\nu \neq 0.5$ within this work.

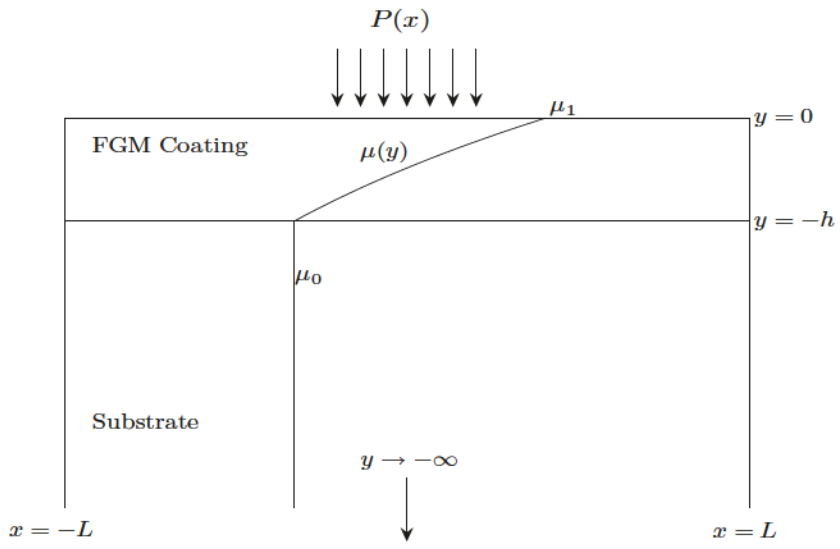

Figure 1: A definition sketch of the problem involving a pressure force applied normally to the solid surface.

A pressure force of the form

$$P(x) = \begin{cases} -p(x), & |x| \leq a, \\ 0, & |x| > a \end{cases} \tag{2}$$

where a denotes the contact half-width is applied normally to the solid surface. The resulting boundary value problem to be solved is then

$$\frac{\partial \sigma_{xx}}{\partial x} + \frac{\partial \sigma_{xy}}{\partial y} = 0, \qquad (-L \leq x \leq L, -\infty < y \leq 0), \tag{3a}$$

$$\frac{\partial \sigma_{xy}}{\partial x} + \frac{\partial \sigma_{yy}}{\partial y} = 0, \qquad (-L \leq x \leq L, -\infty < y \leq 0), \tag{3b}$$

$$\sigma_{yy} - P(x) = 0, \qquad (y = 0), \tag{3c}$$

$$\sigma_{xy} = 0, \qquad (y = 0), \tag{3d}$$

$$\sigma_{xx} = 0, \qquad (x = \pm L), \tag{3e}$$

$$v = 0, \qquad (x = \pm L), \tag{3f}$$

$$|u|, |v| \to 0, \qquad y \to -\infty, \tag{3g}$$

subject to the interfacial matching conditions

$$\sigma_{yy}^{(c)} - \sigma_{yy}^{(s)} = 0, \tag{4a}$$

$$\sigma_{xy}^{(c)} - \sigma_{xy}^{(s)} = 0, \tag{4b}$$

$$u^{(c)} - u^{(s)} = 0, \tag{4c}$$

$$v^{(c)} - v^{(s)} = 0 \tag{4d}$$

applied at $y = -h$. The functions $u(x,y)$ and $v(x,y)$ represent the horizontal and vertical displacements within the solid respectively and the superscripts c and s denote the coating and substrate. The designated boundary conditions specify a frictionless contact on the solid surface and ensure that the coating and substrate are perfectly bonded at their interface. The boundary conditions at $x = \pm L$ and the radiation conditions as $y \to -\infty$ represent the limits in which the applied pressure

ceases to effect the solid. A definition sketch of the contact problem is included in figure (1).

It was shown in Chidlow et al. (2011a) that the displacements induced in the coating can be written as

$$u^{(c)}(x,y) = \sum_{n=1}^{\infty} \xi_n^T(y)\Omega_n \begin{pmatrix} \frac{(1-2\nu)}{2\mu_0}P_n \\ 0 \end{pmatrix} \cos\left(\frac{1}{2}\beta_n(x+L)\right), \tag{5}$$

$$v^{(c)}(x,y) = -\sum_{n=1}^{\infty} \xi_n^T(y)\Gamma_n\Omega_n \begin{pmatrix} \frac{(1-2\nu)}{2\mu_0}P_n \\ 0 \end{pmatrix} \sin\left(\frac{1}{2}\beta_n(x+L)\right) \tag{6}$$

which hold for $-h \leq y \leq 0$ whilst in the substrate

$$u^{(s)}(x,y) = \sum_{n=1}^{\infty} \frac{e^{\frac{1}{2}\beta_n(y+h)}}{\delta_n}\varphi^T(y)\Psi_n \begin{pmatrix} \frac{(1-2\nu)}{2\mu_0}P_n \\ 0 \end{pmatrix} \cos\left(\frac{1}{2}\beta_n(x+L)\right), \tag{7}$$

$$v^{(s)}(x,y) = \sum_{n=1}^{\infty} \frac{e^{\frac{1}{2}\beta_n(y+h)}}{\delta_n}\varphi^T(y)\Phi_n\Psi_n \begin{pmatrix} \frac{(1-2\nu)}{2\mu_0}P_n \\ 0 \end{pmatrix} \sin\left(\frac{1}{2}\beta_n(x+L)\right), \tag{8}$$

which hold for $-\infty < y < -h$. All of the quantities that appear above are defined in the appendix whilst the coefficients P_n in the Fourier series representation of the pressure are defined as

$$\begin{aligned} P_n &= \frac{1}{L}\int_{-L}^{L} P(x)\sin\left(\frac{1}{2}\beta_n(x+L)\right), \\ &= -\frac{1}{L}\int_{-a}^{a} p(x)\sin\left(\frac{1}{2}\beta_n(x+L)\right), \end{aligned} \tag{9}$$

where $\beta_n = n\pi/L$. The stresses within the solid resultant from the applied pressure force may be computed from the displacements u and v using Hooke's laws.

3. Integral equations for the contact problem

The solutions outlined in the previous section give explicit expressions for the horizontal and vertical displacements of a graded elastic solid at any point on or below its surface provided that the contact pressure is known. In many contact problems however, the contact pressure is unknown and instead information about the surface deflection and the nature of the contact (e.g. frictionless, sliding) is given. We show below how the model of the surface deflection given previously can be adapted to formulate integral equations from which the contact pressure can be approximated.

3.1. Recreating the contact pressure when the surface deflection is known

We initially note that the vertical displacement in the coating may be written as

$$v(x,y) = \sum_{n=1}^{\infty} P_n f_n(y)\phi_n(x) \tag{10}$$

where $f_n(y)$ and $\phi_n(x)$ can be easily inferred from (6). In particular, evaluating (10) on the solid surface $y = 0$ gives

$$v(x,0) = \hat{v}(x) = \sum_{n=1}^{\infty} \mathscr{J}_n P_n \phi_n(x), \qquad (-L \le x \le L), \tag{11}$$

with $\mathscr{J}_n = f_n(0)$. Replacing all coefficients P_n appearing in (11) apart from the mth coefficient with their equivalent expressions in (9) yields the first-kind Fredholm integral equation

$$\hat{v}(x) = \mathscr{J}_m P_m \phi_m(x) - \frac{1}{L}\int_{-a}^{a} \sum_{\substack{n=1 \\ n\neq m}}^{\infty} \mathscr{J}_n \phi_n(x)\phi_n(t)p(t)\mathrm{d}t \tag{12}$$

which may be written in operator form as

$$\hat{v}(x) = \mathscr{J}_m P_m \phi_m(x) - \frac{1}{L}(\mathscr{K}_m p)(x). \tag{13}$$

It should be noted that this operator is self-adjoint as the kernel of the integral operator satisfies

$$k_m(x,t) = \sum_{\substack{n=1 \\ n\neq m}}^{\infty} \mathscr{J}_n \phi_n(x)\phi_n(t) = k_m(t,x). \tag{14}$$

We could attempt to approximate the contact pressure $p(x)$ directly from (13). However, the Fourier coefficients P_m appear explicitly in the expressions for the displacements given by (5)-(8) and thus need to be computed during the solution procedure. We therefore choose to directly approximate the coefficients P_m and form the approximation to the applied pressure in terms of its Fourier series.

Assuming that $\hat{v}(x)$ is known throughout $[-a,a]$, we can approximate P_m from (13) using Galerkin's method. This involves considering the weak form of (13) which is attained by multiplying by the functions $\chi_j(x)$, $j = 1,...,M$ and applying the inner product defined as

$$(f,g) = \int_{-a}^{a} f(x)\, g(x) \mathrm{d}x,$$

where f and g are arbitrary functions of x. The weak form of (13) is then

$$(\hat{v},\chi_j) = \mathscr{J}_m P_m(\phi_m,\chi_j) - \frac{1}{L}(\mathscr{K}_m p,\chi_j) \tag{15}$$

which holds for $j = 1,...,M$. At this point, we introduce the approximation to the contact pressure

$$p(x) \approx \sum_{i=1}^{M} b_i \chi_i(x) \tag{16}$$

which is used only within the confines of Galerkin's method to determine P_m. Substituting (16) into (15) then reveals the system of equations

$$(\hat{v},\chi_j) = \mathscr{J}_m P_m(\phi_m,\chi_j) - \frac{1}{L}\sum_{i=1}^{N} b_i(\mathscr{K}_m \chi_i,\chi_j) \tag{17}$$

which may be more conveniently written as

$$V = \mathscr{J}_m P_m \Theta_m - \frac{1}{L} K_m^T b, \tag{18}$$

where

$$b = \left(b_1, b_2, ..., b_M \right)^T, \tag{19}$$

$$V = \left((\hat{v}, \chi_1), (\hat{v}, \chi_2), ..., (\hat{v}, \chi_M) \right)^T, \tag{20}$$

$$\Theta_m = \left((\phi_m, \chi_1), (\phi_m, \chi_2), ..., (\phi_m, \chi_M) \right)^T \tag{21}$$

are column vectors of length M and the $M \times M$ matrix K_m has entries $(K_m)_{ij} = (\mathscr{K}_m \chi_i, \chi_j)$.

Equation (18) relates the unknown coefficients b_i, $i = 1, ..., M$ to the Fourier coefficient P_m and thus comprises $M+1$ unknowns in M equations. An additional equation may be obtained by substituting (16) into (9) which yields

$$P_m = -\frac{1}{L} \Theta_m^T b. \tag{22}$$

Combining (22) with (18) allows us to obtain the approximation

$$P_m = \frac{\Theta_m^T K_m^{-T} V}{1 + \mathscr{J}_m \Theta_m^T K_m^{-T} \Theta_m}. \tag{23}$$

As m is arbitrary, (23) can be used to approximate all of the coefficients in the truncated Fourier series representation of the pressure

$$\begin{aligned} P(x) &= \sum_{m=1}^{N} P_m \phi_m(x), \\ &= \sum_{m=1}^{N} \frac{\Theta_m^T K_m^{-T} V}{1 + \mathscr{J}_m \Theta_m^T K_m^{-T} \Theta_m} \phi_m(x). \end{aligned} \tag{24}$$

which holds for $-L \leq x \leq L$, $N \in \mathbb{N}$.

3.2. Indentation by a rigid punch

In the case of contact between an elastic solid and a rigid punch, the gradient of the surface deflection $\hat{v}'(x)$ rather than the surface deflection itself will be known as the shape of the punch will be given in the problem. In this case, we differentiate (13) with respect to x to give

$$\frac{\partial v}{\partial x}(x,0) = \hat{v}'(x) = J_m P(x)\phi_m'(x) - \frac{1}{L}\int_{-a}^{a} \sum_{\substack{n=1,\\ n\neq m}}^{\infty} \mathscr{J}_n \phi_n'(x)\phi_n(t)p(t)\mathrm{d}t. \tag{25}$$

which can be written in operator form as

$$\hat{v}'(x) = \mathscr{J}_m P_m \phi_m'(x) - \frac{1}{L}(\mathscr{L}_m p)(x) \tag{26}$$

The integral operator $\mathscr{L}_m$ in this case is not self-adjoint as the kernel of the operator $l_m(x,t) \neq l_m(t,x)$.

Utilising Galerkin's method to solve this equation in the same way as before gives the new system

$$F = \mathscr{J}_m P_m \psi_m - \frac{1}{L}\Lambda_m^T b, \tag{27}$$

where

$$F = \left((\hat{v}', \chi_1), (\hat{v}', \chi_2), ..., (\hat{v}', \chi_M)\right)^T, \tag{28}$$

$$\psi_m = \left((\phi_m', \chi_1), (\phi_m', \chi_2), ..., (\phi_m', \chi_M)\right)^T \tag{29}$$

are column vectors of length M and the $M \times M$ matrix Λ_m has entries $(\Lambda_m)_{ij} = (\mathscr{L}_m \chi_i, \chi_j)$. Combining (27) with (22) gives the approximation

$$P_m = \frac{\Theta_m^T \Lambda_m^{-T} F}{1 + \mathscr{J}_m \Theta_m^T \Lambda_m^{-T} \psi_m}. \tag{30}$$

As before this equation holds for arbitrary m and thus we can determine approximations to the coefficients of any required Fourier mode. In this case, the approximation to the applied pressure is taken to be

$$P(x) = \sum_{m=1}^{N} \frac{\Theta_m^T \Lambda_m^{-T} F}{1 + \mathscr{J}_m \Theta_m^T \Lambda_m^{-T} \psi_m} \phi_m(x). \tag{31}$$

which holds in the interval $-L \leq x \leq L$. It should be noted that the punch profile must be smooth, $\hat{v}(x) \in C^1[-a,a]$, in order to ensure that the Fourier series of the pressure converges.

3.3. Choice of trial function

The principal advantage of Galerkin's method is that relatively poor approximations to the contact pressure via (16) will lead to good approximations to the Fourier coefficients P_n, $n \in \mathbb{N}$. The reader is referred to Porter and Stirling (1990) for greater detail.

A good choice of trial function will mimic the behaviour of the true pressure function. In the examples we consider later, the pressure function is known to vanish at the edges of the contact. As a result, we set

$$\chi_j(x) = \sin\left(\frac{j\pi(x+a)}{2a}\right), \qquad j = 1,\ldots,M \tag{32}$$

which has the property that $\chi_j(\pm a) = 0$. Evaluating the functionals appearing in (21) and (29) using this particular choice of trial function gives

$$(\phi_n, \chi_i) = \theta_{i,n} = \begin{cases} \frac{8(-1)^m k\pi a}{(a\beta_{2m})^2 - (2k\pi)^2} \sin\left(\frac{m\pi a}{L}\right), & (i = 2k, n = 2m), \\ \frac{4(-1)^m (2k-1)\pi a}{(a\beta_{2m-1})^2 - ((2k-1)\pi)^2} \cos\left(\frac{(m-\frac{1}{2})\pi a}{L}\right), & (i = 2k-1, n = 2m-1) \\ 0, & \text{otherwise} \end{cases}, \tag{33}$$

and

$$(\phi_n^{'},\chi_i)=\omega_{i,n}=\begin{cases}\frac{4(-1)^m k\pi a\beta_{2m-1}}{(a\beta_{2m-1})^2-(2k\pi)^2}\sin\left(\frac{(m-\frac{1}{2})\pi a}{L}\right), & (i=2k,n=2m-1),\\ \frac{2(-1)^{m+1}(2k-1)\pi a\beta_{2m}}{(a\beta_{2m})^2-((2k-1)\pi)^2}\cos\left(\frac{m\pi a}{L}\right), & (i=2k-1,n=2m),\\ 0, \quad \text{otherwise.}\end{cases} \tag{34}$$

An immediate consequence of these results is that

$$(\mathscr{K}_m\chi_i,\chi_j)=\begin{cases}\sum_{n=1,2n-1\neq m}^{\infty}\mathscr{J}_{2n-1}\theta_{2k-1,2n-1}\theta_{2l-1,2n-1}, & i=2k-1,j=2l-1,\\ \sum_{n=1,2n\neq m}^{\infty}\mathscr{J}_{2n}\theta_{2k,2n}\theta_{2l,2n}, & i=2k,j=2l,\\ 0, \quad \text{otherwise}\end{cases} \tag{35}$$

and

$$(\mathscr{L}_m\chi_i,\chi_j)=\begin{cases}\frac{1}{2}\sum_{n=1,2n-1\neq m}^{\infty}\mathscr{J}_{2n-1}\beta_{2n-1}\theta_{2k-1,2n-1}\omega_{2l,2n-1}, & i=2k-1,j=2l,\\ \frac{1}{2}\sum_{n=1,2n\neq m}^{\infty}\mathscr{J}_{2n}\beta_{2n}\theta_{2k,2n}\omega_{2l-1,2n}, & i=2k,j=2l-1,\\ 0, \quad \text{otherwise}\end{cases} \tag{36}$$

which results in large computational savings as if M is even, there will only be $M^2/2$ non-zero entries in the matrices K_m and Λ_m whilst if M is odd, there will only be $(M^2-1)/2$ non-zero entries in matrix Λ_m and $(M^2+1)/2$ non-zero entries in K_m.

The determination of $(\hat{v}^{'},\chi_j)$ will typically be fairly straightforward as the profile of the punch and thus its gradient will be given as a continuous function making analytical evaluation of the functional simple. The same will not usually be true for the determination of $(\hat{v},\chi_j)$ as the deflection is more likely to be given as a list of discrete values. In this situation, a linear spline (Suli and

Mayers (2003) for example) may be fitted to the data and the functional can be calculated using the piecewise linear function.

4. Numerical Results: Model validation

In this section we verify the accuracy of the solution techniques detailed previously. In all examples given in this paper, the value $L = 10a$ is used to compute results as it was shown in Chidlow et al. (2011a) that this value optimises the balance between computational efficiency and accuracy. Additionally, as we cannot in practise sum an infinite number of terms, all Fourier sums appearing in this work will be truncated at a finite value N. This value will be explicitly stated at the start of each example.

4.1. Example 1: Recreating a known pressure using surface deflection data

We consider the pressure function

$$p(x) = p_0(a^2 - x^2)\left(x + \cos\left(\frac{\pi x}{2a}\right)\right) \tag{37}$$

which is continuous everywhere in $[-a, a]$. Surface deflection data is computed for this pressure using (6) subject to the parameter values $\nu = 0.25$, $\mu_1/\mu_0 = 2$, $h/a = 0.3$ and $N = 200$. In this example, we use (23) and (24) to derive approximations to the surface pressure.

Table (1) compares the exact Fourier coefficients $P_1, ..., P_{10}$ in the series expansion of (37) against approximations computed using (23) by calculating the residual error. The formula used to calculate this quantity is

$$RE = \frac{|P_j - \hat{P}_j|}{P_j} \tag{38}$$

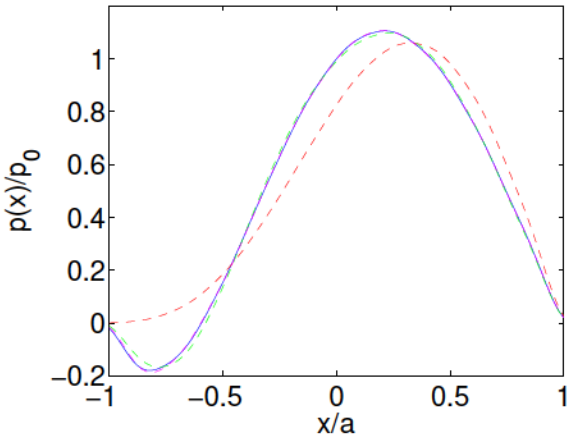

Figure 2: Plots of the approximate pressure curves produced using (23) against the exact pressure given by (37) (blue line). The approximations shown are $M = 2$ (red line), $M = 5$ (green line), $M = 10$ (magenta line).

where $j \in \mathbb{N}$ and $\hat{P}_j$ denotes the approximation to the Fourier coefficient. It can be observed that the residual error in these approximations produced using $M = 2$ is less than 5% whilst when $M = 5$ the error drops to about 1%. As M increases further, the approximations become more and more accurate as expected. In fact the approximate Fourier coefficients are accurate to within 0.01% when a 10 term approximation is used ($M = 10$). Plots of the recreated pressure functions producing using these different values of M are shown in figure (2). It is observed that the approximate pressure curve produced using $M = 5$ agrees almost everywhere with the true pressure curve whilst the approximation computed using $M = 10$ is indistinguishable.

4.2. Example 2: Cylindrical stamp

It has already been seen in the previous example that the integral equation approximation given in this work is highly successful when the surface deflection is known throughout the contact region. We now consider a punch problem to further examine the accuracy of this method.

Residual error in the approximation to the Fourier coefficients P_1-P_{10}					
n	Exact Solution	$M=2$	$M=5$	$M=10$	$M=20$
1	-0.103020	0.018394	3.97×10^{-4}	6.79×10^{-5}	9.71×10^{-6}
2	0.008316	0.048341	0.009019	6.01×10^{-4}	1.107×10^{-4}
3	0.101639	0.013056	2.46×10^{-4}	2.95×10^{-5}	9.83×10^{-6}
4	-0.016284	0.046610	0.008597	6.75×10^{-4}	1.23×10^{-4}
5	-0.098919	0.002315	4.04×10^{-5}	2.02×10^{-5}	1.19×10^{-5}
6	0.023572	0.043696	0.007933	6.36×10^{-4}	1.27×10^{-4}
7	0.094948	0.014050	4.634×10^{-4}	1.05×10^{-4}	4.21×10^{-5}
8	-0.029886	0.039383	0.006993	5.35×10^{-4}	1×10^{-4}
9	-0.089849	0.036316	9.9×10^{-4}	2.22×10^{-4}	7.79×10^{-5}
10	0.034987	0.033670	0.005774	4.86×10^{-4}	1.43×10^{-4}

Table 1: A comparison of the residual error in the approximation to the first 10 coefficients $P_1,...,P_{10}$ appearing in the Fourier representation of (37) compared with approximations computed using (23) for different values of M.

Consider indenting the surface of the solid by a rigid cylindrical stamp. The stamp profile is approximated using a parabola so that the deflection on the solid surface is given as

$$\hat{v} = -\varepsilon_0 + \frac{x^2}{2R} \tag{39}$$

where R is the radius of the stamp and ε_0 is an as yet unknown constant which denotes the maximum deflection of the solid surface. It is easily seen here that

$$\hat{v}' = \frac{x}{R} \tag{40}$$

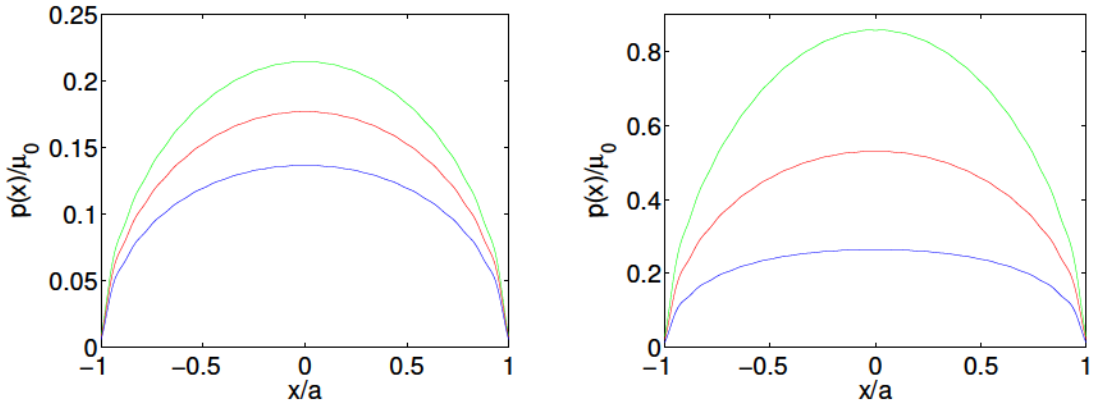

(a) $h/a = 10$ (b) $h/a = 10/3$

Figure 3: Plots of the dimensionless contact pressure curves produced for the cylindrical punch in example 2. The approximations shown are $\mu_1/\mu_0 = 8$ (blue line), $\mu_1/\mu_0 = 1.0001$ (red line), and $\mu_1/\mu_0 = 1/8$ (green line).

and thus

$$(\hat{v}', \chi_j) = \begin{cases} -\frac{2a^2}{k\pi R}, & (j = 2k), \\ 0, & (j = 2k-1) \end{cases} \tag{41}$$

for the trial functions defined in (32).

It is our intention in this example to recreate the results of Ke and Wang (2006). In order to do this, we take $M = 30$, $N = 400$, $\nu = 0.3$, $R/h = 0.8$ and plot the dimensionless contact pressure $p(x)/\mu_0$ for three different coatings: $\mu_1/\mu_0 = 8, 1, 1/8$ subject to the relative thicknesses $h/a = 10, 10/3$. It should be noted that the contact model used in this paper is not valid for a homogeneous solid and thus in order to compare with the homogeneous solution of Ke and Wang, we take the stiffness ratio to be almost but not identically 1 (the actual value is $\mu_1/\mu_0 = 1.0001$). The results produced for this problem are depicted in figure (3) and show excellent agreement with those given by Ke and Wang (2006) (compare with their figure 9).

5. The full contact problem

It has been tacitly assumed in the previous sections that the contact half-width is given as part of the problem. Unfortunately in many real problems this is not the case and typically a will need to be determined as part of the solution procedure.

If the contact half-width is not known in advance of the problem, the total load W applied to the solid surface will be given. The load is defined as

$$W = -\int_{-L}^{L} P(x)\mathrm{d}x, \tag{42}$$

$$= \int_{-a}^{a} p(x)\mathrm{d}x \tag{43}$$

which following simple integration of (24) may be written as

$$W = 4\sum_{n=1}^{\infty} \frac{(-1)^n P_{2n-1} \sin\left(\frac{1}{2}a\beta_{2n-1}\right)}{\beta_{2n-1}}. \tag{44}$$

As it is known that the contact region increases in size as the total load increases, we deduce that

1) $W(a)$ is a monotically increasing function,

2) each value of a gives rise to a unique total load for fixed material parameters (ν, μ_0, μ_1, h).

This information allows us to formulate an iterative algorithm to compute a.

Define the function $f(a)$ as

$$f(a) = W - 4\sum_{n=1}^{\infty} \frac{(-1)^n P_{2n-1} \sin\left(\frac{1}{2}(a\beta_{2n-1})\right)}{\beta_{2n-1}} \tag{45}$$

which will be identically zero if a is equivalent to the contact half-width. By choosing some initial guess a_0 to approximate a, we can use the secant method to update each guess and calculate the

true contact half-width. The iterative formula used here is then

$$a_{j+1} = a_j - \frac{\delta_a f(a_j)}{f(a_j+\delta_a) - f(a_j)}, \tag{46}$$

for some $\delta_a > 0$ and $j = 1, 2, \ldots$. It is anticipated that the value of a will typically be very small in the vast majority of problems and thus a direct measure of the difference between a_{j+1} and a_j could potentially give a misleading estimate of the accuracy of the approximation to a. A better choice is to stipulate that the true value of a is obtained when the criterion

$$\frac{|a_{j+1} - a_j|}{|a_{j+1}|} < \varepsilon_a \tag{47}$$

is met. This ensures that high accuracy in the approximation to a is achieved regardless of its magnitude.

The solution procedure in full is then to calculate P_m, $m \in \mathbb{N}$ using either (23) or (30) (depending on the problem) for each value of a_j, determine $f(a_j)$ and $f(a_j+\delta)$ and update the approximation to a using (46) until the contact half-width is found to a desired accuracy. A flowchart outlining the steps in the solution procedure is given in figure (4).

5.1. Example

We test the iterative method proposed in this section by considering a more realistic problem. A rigid cylindrical stamp of radius 5cm and length 10cm makes contact with the surface of an inhomogeneous solid which comprises a substrate made of steel ($\nu = 0.3$, Young's modulus $E_1 = 1 \times 10^{11}$Pa). The applied load resulting from the contact is 100N.

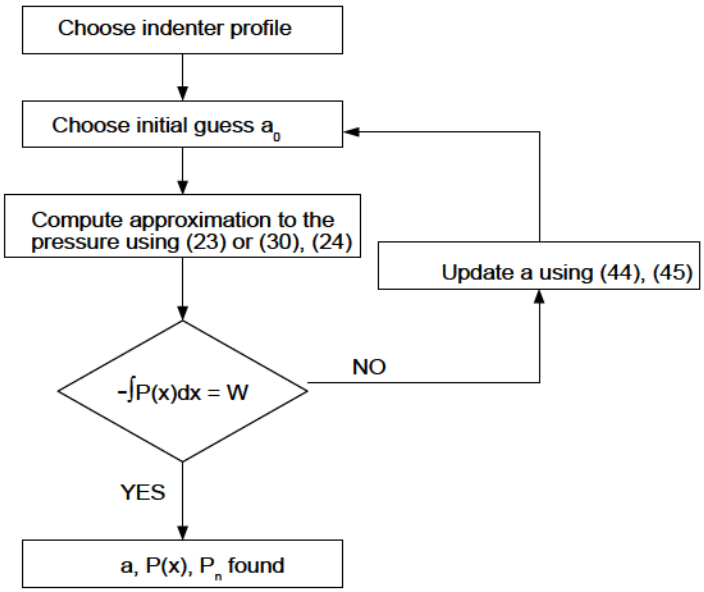

Figure 4: The steps in the iterative algorithm used to determine the contact half-width a and pressure $p(x)$.

Our aim in this example is to consider how the inhomogeneity of the coating affects the predicted pressure curves. This may be achieved by comparing the predicted results for both hard and soft coatings with those predicted by Hertzian theory. The contact half-width and maximum pressure predicted from Hertzian theory are

$$a_{\mathrm{h}} = \sqrt{\frac{2WR(1-\nu)}{\pi\mu_1}}, \qquad p_{\mathrm{h}} = \frac{2W}{\pi a_{\mathrm{h}}}$$

which in this example give $a_{\mathrm{h}} = 5.382\mu\mathrm{m}$ and $p_{\mathrm{h}} = 1.182 \times 10^7\mathrm{Pa}$. Unlike in our previous examples, the contact half-width is not known in advance of the solution and thus we cannot fix the relative coating thickness h/a. Instead, we choose here to fix the ratio h/a_{h}. It should also be noted that we take $N = 800$ and $\delta_a = \varepsilon_a = 1 \times 10^{-7}$ in this example.

Figure (5) depicts the predicted pressure curves for a selection of different coatings subject to two different relative thicknesses h/a_h. It is observed that the pressure curves for the harder coat-

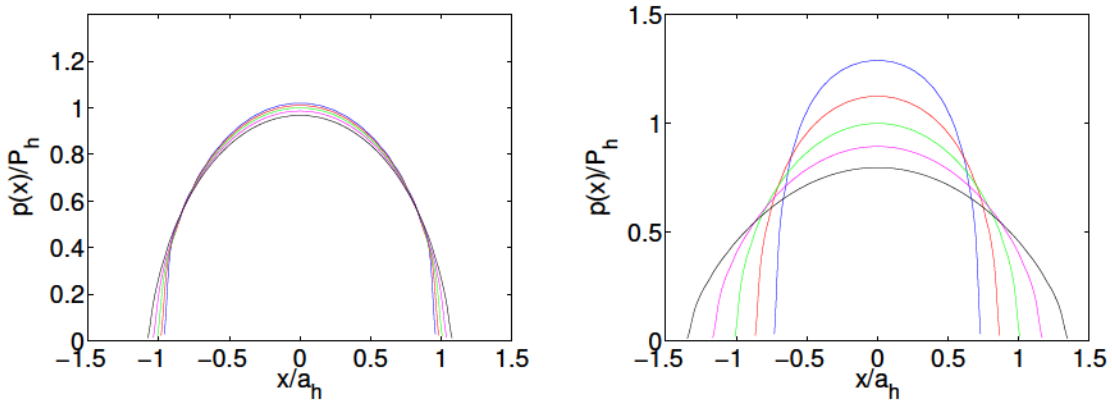

(a) $h/a_{\mathrm{h}} = 0.1$ (b) $h/a_{\mathrm{h}} = 1$

Figure 5: Plots of the predicted contact pressures induced within example 3 for two representative coating thicknesses. The approximations shown are $\mu_1/\mu_0 = 4$ (blue line), $\mu_1/\mu_0 = 2$ (red line), $\mu_1/\mu_0 = 1.0001$ (green line), $\mu_1/\mu_0 = 1/2$ (magenta line) and $\mu_1/\mu_0 = 1/4$ (black line).

ings give rise to larger maximum pressures and smaller contact half-widths than those predicted by Hertzian pressure whilst softer coatings produce smaller maximum pressures and larger contact half-widths. These observations become more marked as the ratio h/a_{h} increases as can be seen in figure (5b).

It has been noted in figure (5) that although material inhomogeneity certainly leads to departures from the predictions of Hertzian pressure, the differences are less marked as the ratio h/a_{h} decreases. In order to more fully consider this phenomenon, we see how the dimensionless predicted maximum pressure $p_{\max}/p_{\mathrm{h}}$ and dimensionless contact half-width a/a_{h} changes as the ratio h/a_{h} increases. These results are presented in figure (6) and it is seen that as the ratio h/a_{h} increases, the predicted maximum pressures and contact half-widths for both harder and softer coatings diverge further and further from the Hertzian predictions. Conversely, when h/a_{h} is small, the results predicted for the inhomogeneous materials are similar to those predicted using

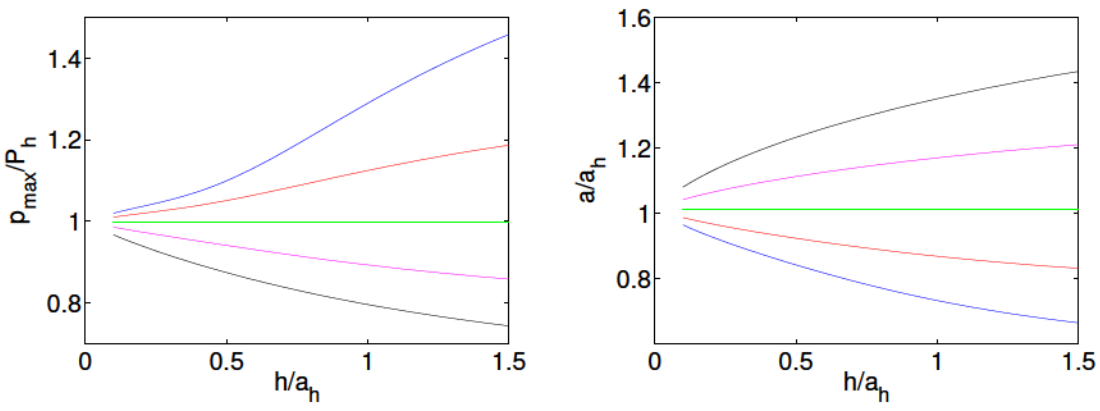

(a) (b)

Figure 6: The evolution of a) the dimensionless maximum pressure and b) the dimensionless contact radii for a selection of graded elastic coatings as h/a_h changes. The key used is identical to that in figure (5).

Hertzian theory. We can deduce that Hertzian theory may be used to determine solutions to the contact problem in the limit $h/a_{\mathrm{h}} \to 0$ with a reasonable degree of accuracy. As the relative coating thickness becomes larger, other methods must be sought to provide accurate solutions.

An alternate way of investigating the limitations of Hertzian theory is to calculate the sub-surface stress field that results from the applied surface pressure. The choice is made here to consider the Tresca principal stress field which may be defined at any point as

$$\tau_1 = \frac{1}{2}\sqrt{(\sigma_{xx}-\sigma_{yy})^2+4\sigma_{xy}^2}. \tag{48}$$

Please note that all of the sub-surface stress fields considered within this paper will be of Tresca type and that the contour plots are non-dimensionalised with respect to the maximum Hertzian pressure p_h so that the results presented depict τ_1/p_h.

The non-dimensional sub-surface stress fields produced for the control case $\mu_1/\mu_0 = 1.0001$ and the hard and soft coatings $\mu_1/\mu_0 = 0.5, 2$ subject to the two relative thicknesses $h/a_h = 0.1, 1$

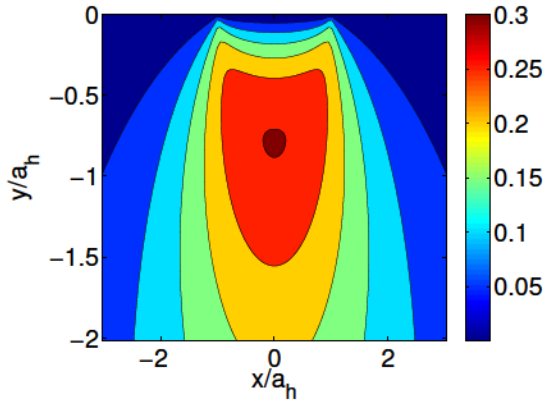

(a) $\mu_1/\mu_0 = 1.0001$

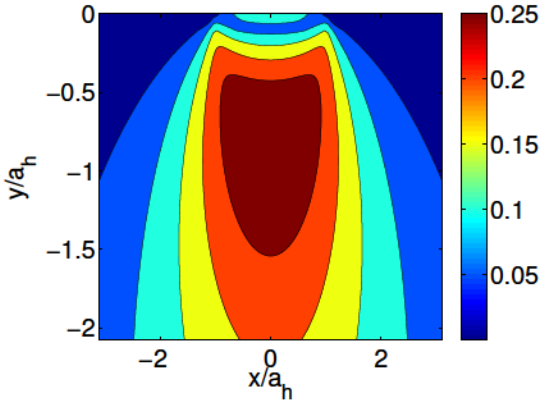

(b) $\mu_1/\mu_0 = 0.5, h/a_h = 0.1$

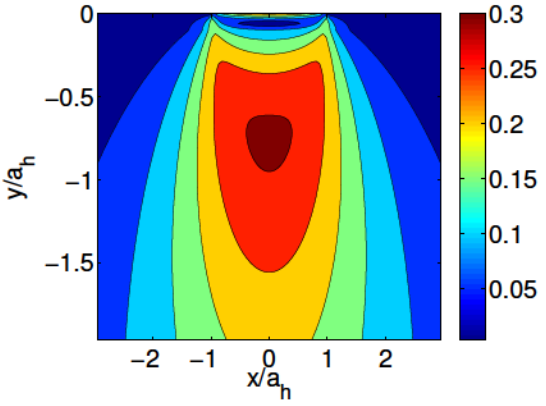

(c) $\mu_1/\mu_0 = 2, h/a_h = 0.1$

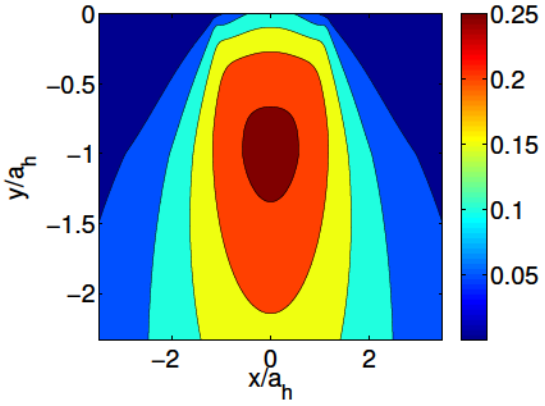

(d) $\mu_1/\mu_0 = 0.5, h/a_h = 1$

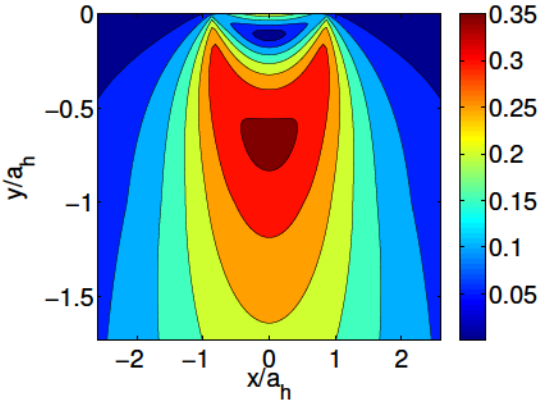

(e) $\mu_1/\mu_0 = 2, h/a_h = 1$

Figure 7: Dimensionless principal stresses τ_1/p_h for a) the control case $\mu_1/\mu_0 = 1.0001$, b) a thin soft coating, c) a thin hard coating, d) a thick soft coating and e) a thick hard coating.

are presented in figure (7). It may be seen that the stress field produced for the control case in figure (7a) agrees very closely with the results obtained from the Hertzian pressure distribution (see Johnson (1985) for example). We find in this case that $\tau_{\max}/p_h = 0.301$ which occurs when $y/a_h = -0.796$. These values agree well with those given by Hertzian theory.

The results presented in figures (7b-c) indicate that when the coating is thin, the sub-surface stress fields obtained for the inhomogeneous solids are very similar to that of the control case. It is found here that for $\mu_1/\mu_0 = 2$, $\tau_{\max}/p_h = 0.306$ and for $\mu_1/\mu_0 = 0.5$, $\tau_{\max}/p_h = 0.297$ which occur when $y/a_h = -0.768$ and $y/a_h = -0.808$ respectively. These results are not dissimilar to those given by Hertzian theory.

We observe in figures (7d-e) that as the coating becomes relatively thick, the stress fields produced for the hard and soft coating differ dramatically from those produced for the control case. It is seen here that a large concentration of stress close to the solid surface is present in the softer coating whilst there is a region of very low stress occurring immediately below the surface in the harder coating. It is also found in this situation that when $\mu_1/\mu_0 = 2$, $\tau_{\max}/p_h = 0.359$ whilst when $\mu_1/\mu_0 = 0.5$, $\tau_{\max}/p_h = 0.262$ which occur at $y/a_h = -0.687$ and $y/a_h = -1.010$ respectively. These results reaffirm our conclusion that Hertzian theory is unable to provide accurate solutions to the contact problem involving inhomogeneous materials outside of the limit $h/a_h \to 0$.

The observations made in this example about the behaviour of the maximum principal stresses are potentially significant in the determination of material failure. We have seen that under a fixed load, hard coatings experience a larger maximum principal stress than soft coatings. This trend becomes more exaggerated as the ratio h/a_h increases which indicates that hard coatings become

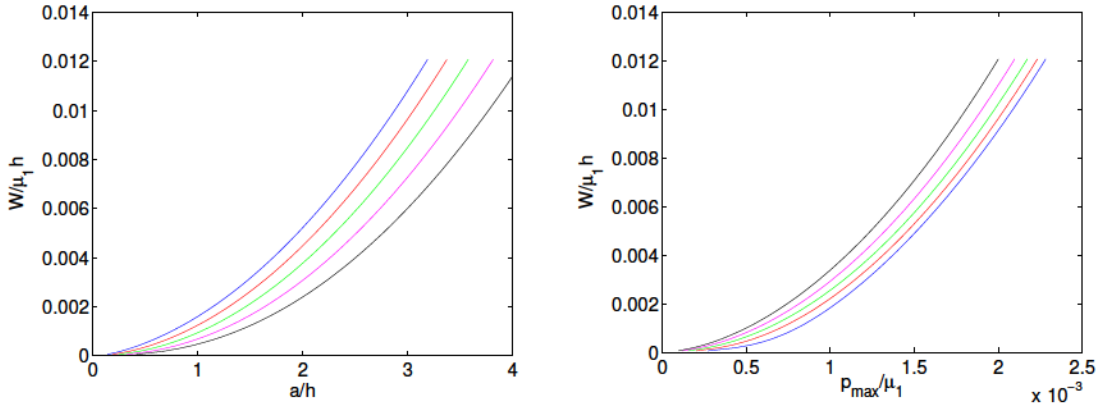

(a) (b)

Figure 8: Plots of the evolution of the dimensionless contact half-width a/h and maximum contact pressure $p_{\max}$ vs the dimensionless load $W/\mu_0 h$. The key used here is the same as that in figure (5).

increasingly more likely to experience plastic flow as coating thickness increases whilst softer materials are less likely to fail. A more detailed discussion about the behaviour of the maximum principal stresses is contained within Chidlow et al. (2011a).

As we have considered the behaviour of the maximum contact pressure, contact-half width and principal stress under fixed load, we now investigate how these parameters behave when the applied load is allowed to vary. In this situation we cannot non-dimensionalise the parameters in the same way as before as the contact half-width and maximum pressure predicted using Hertzian theory are load-dependent. Instead we consider how the dimensionless quantities h/a and $p_{\max}/\mu_0$ vary with $\bar{W} = W/\mu_0 h$. These results are plotted in figure (8) and indicate that whilst a and $p_{\max}$ both increase with the load, the relationships are not linear (Guler and Erdogan (2007) suggest that this relationship is approximately parabolic but please note when comparing results that our non-dimensionalisation of the load and contact half-width is different to theirs). We further note that under equivalent loads, the contact half-width is larger in magnitude for softer coatings than

harder coatings whilst the maximum pressure is larger for harder coatings. These observations reaffirm our earlier conclusions.

6. Adhesive contacts

We now show how to modify the proposed solution algorithm in this work to solve problems of adhesive contact between a graded elastic solid and rigid punch. The vast majority of research conducted on the subject of adhesive contacts has involved homogeneous materials and as such is likely to be of limited use when studying adhesive contact problems involving inhomogeneous materials. The aim of this section is therefore to conduct a preliminary investigation into adhesive contact problems involving FGMS.

6.1. Integral equation formulation

Following the assumption of Maugis (1992) that adhesive forces outside of the contact are constant, we take the total pressure applied to the solid surface as

$$P(x) = \begin{cases} \sigma_0, & -c \le x \le -a \\ -\hat{p}(x), & -a \le x \le a, \\ \sigma_0, & a \le x \le c, \\ 0, & \text{otherwise.} \end{cases} \tag{49}$$

where $\sigma_0 = \Delta\gamma/Z_0$, $\Delta\gamma$ is the work of adhesion (also called the Dupre surface energy) and $Z_0(>0)$ is the critical gap width at which the attractive forces between the solid and punch fall to zero. This critical gap width occurs at $x = c$. We note in this problem that $\hat{p}(x)$ will be a combination of both

adhesive and contact forces and satisfies

$$\hat{p}(-a) = -\sigma_0, \tag{50}$$

$$\hat{p}(a) = -\sigma_0 \tag{51}$$

which ensures continuity of $P(x)$. A definition sketch of the adhesive contact problem is contained in figure (9).

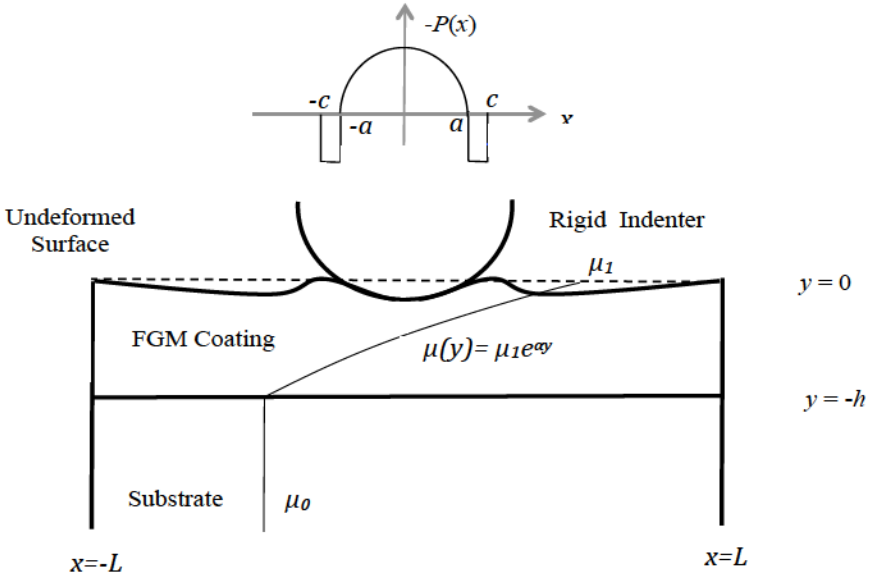

Figure 9: A definition sketch of the adhesive contact problem.

At this point we introduce the parameter

$$\lambda = \sigma_0 \left(\frac{R(1-\nu^2)^2}{\Delta\gamma\mu_1^2} \right)^{\frac{1}{3}}, \tag{52}$$

which has been used extensively (see Johnson and Greenwood (2008) for example) to characterise adhesive behaviour in homogeneously elastic contact problems. We make reference to this parameter later to try and characterise adhesive behaviour in inhomogeneously elastic contact problems.

We note in this problem that a much greater number of modes will be required to accurately represent $P(x)$ as a Fourier series as it will have slope discontinuities at both $x = \pm a$ and is discontinuous at $x = \pm c$. In this situation, the previous formula used to evaluate P_m (30) becomes inconvenient to use because the evaluation of the matrix Λ_m for each m involves a high computational cost. We outline an alternate method here from which the Fourier coefficients P_m can be more efficiently calculated.

Substituting (9) into (10) allows us to construct the integral equation

$$\hat{v}'(x) = \frac{1}{L}\sum_{n=1}^{\infty} \mathscr{J}_n \int_{-L}^{L} P(t)\phi_n(t)\phi_n'(x)\mathrm{d}t \tag{53}$$

which holds everywhere in $[-L, L]$. Use of (49) then yields

$$\begin{aligned}\hat{v}'(x) &= \frac{1}{L}\sum_{n=1}^{\infty} \mathscr{J}_n \left(\sigma_0 \left(\int_{-c}^{-a} \phi_n(t)\mathrm{d}t + \int_{a}^{c} \phi_n(t)\mathrm{d}t\right) - \int_{-a}^{a} \hat{p}(t)\phi_n(t)\mathrm{d}t\right)\phi_n'(x), \\ &= \sum_{n=1}^{\infty} \mathscr{J}_n \left(\zeta_n - \frac{1}{L}\int_{a}^{a} \hat{p}(t)\phi_n(t)\mathrm{d}t\right)\phi_n'(x)\end{aligned} \tag{54}$$

where

$$\zeta_n = \frac{\sigma_0}{L}\left(\int_{-c}^{-a} \phi_n(t)\mathrm{d}t + \int_{a}^{c} \phi_n(t)\mathrm{d}t\right), \tag{55}$$

$n \in \mathbb{N}$. As the coefficients ζ_n involve only known quantities, they can be determined in advance of the problem and hence serve only to modify the forcing term within the integral equation. As a consequence, we may write the above integral equation as

$$\hat{v}'(x) - \sum_{n=1}^{\infty} \mathscr{J}_n \zeta_n \phi_n'(x) = -\frac{1}{L}\sum_{n=1}^{\infty} \mathscr{J}_n \int_{-a}^{a} \hat{p}(t)\phi_n(t)\phi_n'(x)\mathrm{d}t, \tag{56}$$

which holds $\forall x \in [-L, L]$. This equation may be solved as before using Galerkin's method with the exception that the trial functions previously used in the initial approximation given by (32) cannot

be used as they will return a very poor approximation to $\hat{p}(x)$ near the edges of the contact as they satisfy $\chi_j(\pm a) = 0$, $j = 1,...,M$. This difficulty may be overcome by defining the new function

$$Q(t) = \hat{p}(t) + \sigma_0, \qquad -a \leq t \leq a \tag{57}$$

which satisfies $Q(\pm a) = 0$. Substituting (57) into (56) gives the new equation

$$\hat{v}'(x) - \sum_{n=1}^{\infty} \mathscr{J}_n \rho_n \phi_n'(x) = -\frac{1}{L} \sum_{n=1}^{\infty} \mathscr{J}_n \int_{-a}^{a} Q(t)\phi_n(t)\phi_n'(x)\mathrm{d}t \tag{58}$$

where

$$\rho_n = \frac{\sigma_0}{L} \int_{-c}^{c} \phi_n(t)\mathrm{d}t. \tag{59}$$

Multiplying (58) by the test functions $\chi_j(x)$ and integrating over the contact area gives the system

$$(\hat{v}', \chi_j) - \sum_{n=1}^{\infty} \mathscr{J}_n \rho_n (\phi_n', \chi_j) = -\frac{1}{L}(\mathscr{L}Q, \chi_j), \qquad j = 1,...,M. \tag{60}$$

Introducing the approximation

$$Q(x) \approx \sum_{i=1}^{M} b_i \chi_i(x) \tag{61}$$

into (60) then gives the system

$$G = -\frac{1}{L}\Delta^T b \tag{62}$$

which may be rearranged to give

$$b = -L\Delta^{-T} G. \tag{63}$$

The vectors used above are defined as

$$G = \Big((g,\chi_1), (g,\chi_2), ..., (g,\chi_M) \Big)^T, \tag{64}$$

$$b = \Big(b_1, b_2, ..., b_M \Big)^T \tag{65}$$

with

$$g(x) = \hat{v}'(x) - \sum_{n=1}^{\infty} \mathscr{J}_n \rho_n \phi_n'(x), \tag{66}$$

whilst $\Delta_{ij} = (\mathscr{L}\chi_i, \chi_j)$, $i, j = 1, ..., N$. The Fourier coefficients P_n can then be computed from the formula

$$\begin{aligned} P_n &= -\frac{1}{L}\int_{-a}^{a} (Q(x) - \sigma_0)\,\phi_n(x)\mathrm{d}x + \zeta_n, \\ &= -\frac{1}{L}\sum_{i=1}^{M} b_i(\chi_i, \phi_n) + \frac{\sigma_0}{L}\int_{-c}^{c} \phi_n(x)\mathrm{d}x, \\ &= -\frac{1}{L}\sum_{i=1}^{M} b_i\theta_{i,n} + \frac{4\sigma_0}{n\pi}\sin\left(\frac{\beta_n L}{2}\right)\sin\left(\frac{\beta_n c}{2}\right) \end{aligned} \tag{67}$$

with $\theta_{i,n}$ given by (33) as before. This expression may be simplified to finally give

$$P_n = \begin{cases} -\frac{1}{L}\sum_{i=1}^{M} b_i\theta_{i,2m}, & (n = 2m), \\ -\frac{1}{L}\sum_{i=1}^{M} b_i\theta_{i,2m-1} + \frac{4\sigma_0}{(2m-1)\pi}(-1)^{m+1}\sin\left(\frac{\beta_{2m-1}c}{2}\right), & (n = 2m-1). \end{cases} \tag{68}$$

Many practical problems involving adhesive contacts will require the determination of both a and c. The iterative algorithm proposed in section (5) may still be used here to determine the contact half-width with a slight-modification which we discuss shortly. The value of c however needs to be computed using other means. The next section details an efficient iterative solver which may be used to compute this value.

6.2. Determining c: the case of a cylindrical punch

The point c represents the location at which the critical gap Z_0 occurs. If we let $\xi(x)$ denote the gap at any point between the solid surface and the indenter, we see from its definition that

$\xi(c) = Z_0$. In the case of contact by a cylindrical punch, we may use (11) and (39) to write

$$\xi(x) = \text{abs}\left(-\varepsilon_0 + \frac{x^2}{2R} - \sum_{n=1}^{\infty} \mathscr{J}_n P_n \phi_n(x)\right) \tag{69}$$

so that

$$Z_0 = \text{abs}\left(-\varepsilon_0 + \frac{c^2}{2R} - \sum_{n=1}^{\infty} \mathscr{J}_n P_n \phi_n(c)\right). \tag{70}$$

The absolute value is used in (69) and (70) to ensure that the obtained gap-width is always positive. We note that the maximum penetration depth $-\varepsilon_0$ will occur at the origin in this case and will be given by the formula

$$-\varepsilon_0 = \sum_{n=1}^{\infty} \mathscr{J}_n P_n \phi_n(0), \tag{71}$$

thus allowing us to write (70) as

$$Z_0 = \text{abs}\left(\frac{c^2}{2R} + \sum_{n=1}^{\infty} \mathscr{J}_n P_n \big(\phi_n(0) - \phi_n(c)\big)\right). \tag{72}$$

This equation may be solved iteratively in an identical way to the contact half-width a by using the secant method. Defining the function

$$\eta(c) = \text{abs}\left(\frac{c^2}{2R} + \sum_{n=1}^{\infty} \mathscr{J}_n P_n \big(\phi_n(0) - \phi_n(c)\big)\right) - Z_0 \tag{73}$$

allows us to choose an initial guess c_0 to c and iterate using the formula

$$c_{i+1} = c_i - \frac{\delta_c \eta(c_i)}{\eta(c_i + \delta_c) - \eta(c_i)} \tag{74}$$

for $i \geq 0$. As before, we deem that the true value of c has been found when

$$\frac{|c_{i+1} - c_i|}{|c_{i+1}|} < \varepsilon_c. \tag{75}$$

6.3. Re-computing the contact half-width

In the case of adhesive contact considered here, the pressure applied to the solid surface is non-zero in the interval $(-c,c)$. Using (42), we see here that

$$\begin{aligned} W &= -\int_{-L}^{L} P(x)\mathrm{d}x, \\ &= -\left(2\sigma_0\int_a^c \mathrm{d}x - \int_{-a}^{a}\hat{p}(x)\mathrm{d}x\right), \\ &= \int_{-a}^{a}\hat{p}(x)\mathrm{d}x - 2\sigma_0(c-a). \end{aligned} \tag{76}$$

This may be written in series form as

$$W = 4\sum_{n=1}^{\infty}\frac{(-1)^n P_{2n-1}\sin\left(\frac{1}{2}(c\beta_{2n-1})\right)}{\beta_{2n-1}} \tag{77}$$

which follows from (44). Using this new expression for the load in (45) and (46) allows us to compute a iteratively as before. Note that although a does not explicitly appear in (77), all quantities appearing in this equation are a-dependent.

A flowchart of the steps used to solve the adhesive circular punch problem is contained in figure (10). It should be noted that this solution technique may be used to determine c in cases of contact with arbitrary shaped punches. The only modification necessary is the insertion of the desired profile into (70).

We use the initial guesses $a_0 = c_0 = a_h$ within this work as this value can be computed easily from an explicit formula. Another possible choice would be to use the value of c computed from Johnson and Greenwood (2008) but this requires further iterative calculations and is thus not used here.

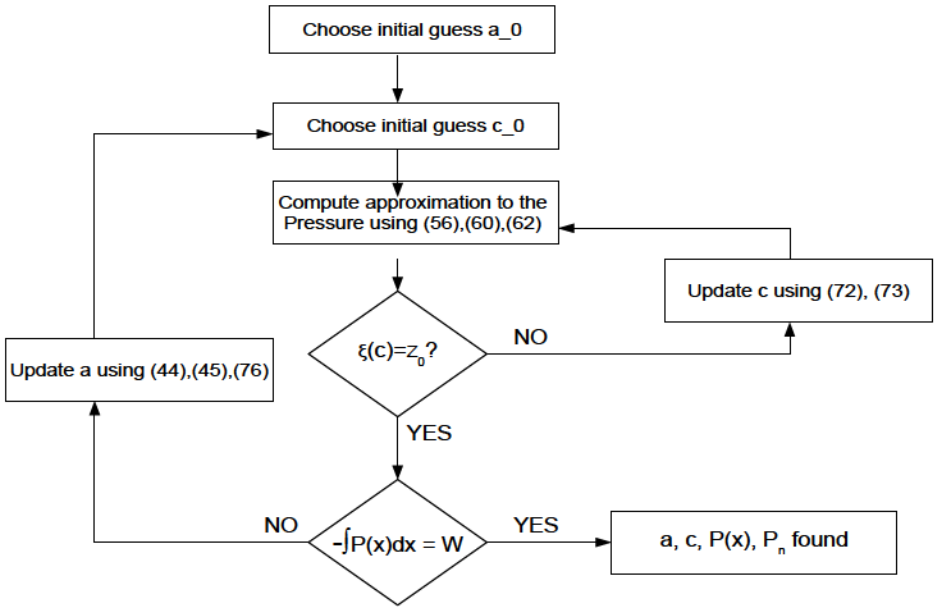

Figure 10: An outline of the method used to determine the solution of adhesive contact problems

7. Example: Adhesive circular punch

We conclude this work with an example of an adhesive contact problem. A graded elastic solid is contacted by a rigid circular punch of radius $5\mu m$ and length $10\mu m$ with a resultant load of 200N. The Poisson ratio of the solid is taken to be 0.23 whilst the shear modulus of the substrate is 1×10^9Pa. The critical gap-width at which there ceases to be adhesion between the punch and the solid is 3.51nm. As this value is of $O(10^{-9})m$, we choose $\delta_a = \delta_c = 1 \times 10^{-12}$ and $\varepsilon_a = \varepsilon_c = 1 \times 10^{-6}$ here. We additionally choose $N = 2000$ to produce results for soft coatings $(\mu_1/\mu_0 < 1)$ and $N = 3000$ to produce results for hard coatings $(\mu_1/\mu_0) > 1$.

Our main objective within this example will be to determine the effects the parameter λ and the relative coating thickness h/a_h have on $\hat{p}(x)$, a, c and the Tresca-type sub-surface stress field. Plots of the evolution of the parameters a and c in this problem for $0.3 \leq \lambda \leq 3$ are presented in

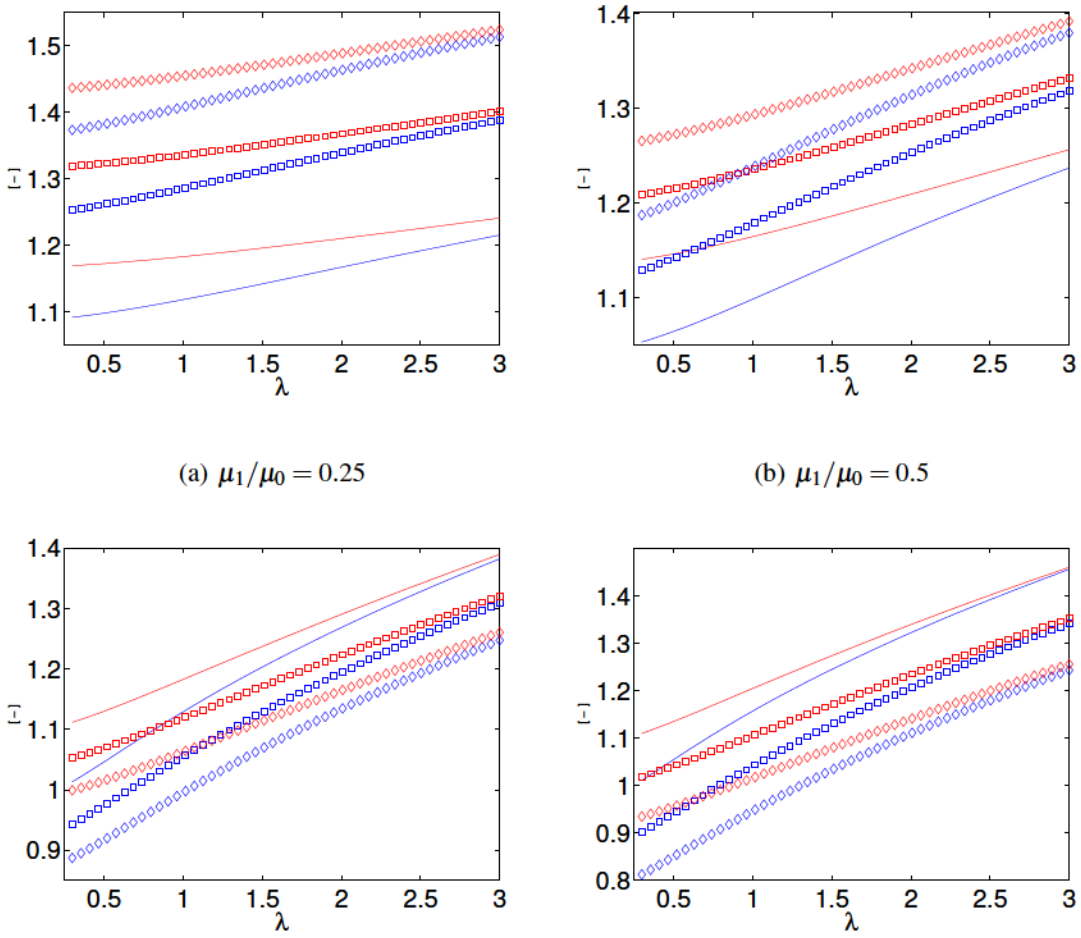

(a) $\mu_1/\mu_0 = 0.25$

(b) $\mu_1/\mu_0 = 0.5$

(c) $\mu_1/\mu_0 = 2$

(d) $\mu_1/\mu_0 = 3$

Figure 11: The evolution of the dimensionless parameters a/a_h (blue lines) and c/a_h (red lines) for four different coatings of three different thicknesses. The solid lines represent $h/a_h = 0.1$, the squares represent $h/a_h = 0.5$ and the diamonds represent $h/a_h = 1$.

figure (11). We can immediately see for the soft coatings in figures (11a) and (11b) that as the value of λ increases, both a/a_h and c/a_h increase in magnitude. We also see that both parameters start to coalesce as λ increases which indicates that the band width $c-a$ over which adhesion occurs decreases. This observation is in accord with those of Johnson and Greenwood (2008) for a homogeneous solid. It is of further interest to note that as the relative coating thickness h/a_h increases, the magnitude of both a/a_h and c/a_h increase as well. This indicates that as the contact becomes more adhesive, the predicted contact half-width of Hertz becomes less and less accurate as it significantly underestimates the true value.

The behaviour of a/a_h and c/a_h for the harder coatings satisfying $\mu_1/\mu_0 = 2$ and $\mu_1/\mu_0 = 3$ are presented in figures (11c) and (11d). We can immediately see here that both a/a_h and c/a_h increase in magnitude and begin to coalesce as λ increases. These characteristics are in accord with those observed for the softer coatings in (11a) and (11b). We notice here however that the values of a/a_h and c/a_h decrease in magnitude as the relative coating thickness increases in magnitude. This is a complete contrast to the observed behaviour for soft coatings as it indicates that the area over which pressure is applied to the solid surface decreases as h/a_h increases. We note however that this behaviour agrees well with the trends that were previously seen in figure (5).

It is of further interest to determine how the dimensionless maximum contact pressure $\hat{p}_{\max}$ is affected by both λ and h. Table (2) presents the maximum pressures applied on the solid surface for a selection of different coatings subject to different relative thicknesses h/a_h and values of λ. We can immediately see from these results that the coating thickness has a significant effect on the value of the maximum pressure. The two softer coatings experience a significant decrease in the

maximum applied pressure as the value of h/a_h increases whilst the two harder coatings experience a significant increase in the maximum applied pressure. However, we also note that subject to a fixed value of h/a_h, an increase in λ makes almost no difference to the predicted maximum pressure obtained for each different coating. This indicates that increased work of adhesion has virtually no effect on the maximum pressure experienced during contact, an observation made by Johnson and Greenwood (2008) for the homogeneous case.

The predicted maximum pressure for a selection of different coatings and thicknesses					
λ	h/a_h	$\mu_1/\mu_0 = 0.25$	$\mu_1/\mu_0 = 0.5$	$\mu_1/\mu_0 = 2$	$\mu_1/\mu_0 = 3$
0.3	0.1	0.9622	0.9836	1.0152	1.0242
	0.5	0.8614	0.9337	1.0634	1.0997
	1	0.7837	0.8857	1.1392	1.2402
1	0.1	0.9639	0.9870	1.0283	1.0435
	0.5	0.8628	0.9369	1.0759	1.1177
	1	0.7849	0.8886	1.1531	1.2603
2	0.1	0.9674	0.9938	1.0534	1.0794
	0.5	0.8659	0.9434	1.1011	1.1525
	1	0.7874	0.8946	1.1792	1.2956
3	0.1	0.9718	1.0019	1.0795	1.1163
	0.5	0.8696	0.9514	1.1295	1.1872
	1	0.7907	0.9022	1.2078	1.3330

Table 2: The predicted maximum pressure $\hat{p}_{\max}$ for four coatings satisfying $\mu_1/\mu_0 = 0.25, 0.5, 2, 3$. Each coating is considered at three different thicknesses $h/a_h = 0.1, 0.5, 1$ and subject to four different values of λ.

We conclude this section by considering the behaviour of the sub-surface stress (Tresca) fields and total pressures produced for the soft coating $\mu_1/\mu_0 = 0.5$ and hard coating $\mu_1/\mu_0 = 2$ with $h/a_h = 0.5$ subject to four different values of λ. Figure (12) shows the total pressure forces acting on the solid in this example. It is readily observed that the results produced for both the hard and

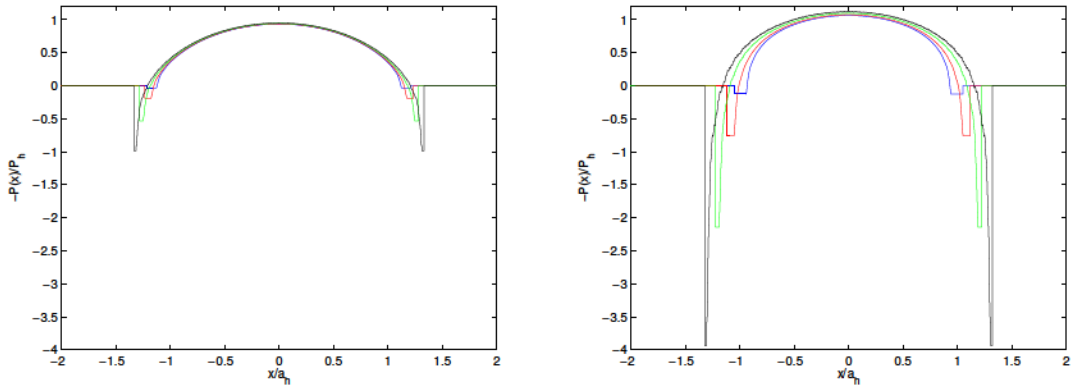

(a) $\mu_1/\mu_0 = 0.5$ (b) $\mu_1/\mu_0 = 2$

Figure 12: The total pressure applied to the solid in the adhesive punch problems for two different coatings. The blue line represents $\lambda = 0.3$, the red line $\lambda = 1$, the green line $\lambda = 2$ and the black line $\lambda = 3$.

soft coating are qualitatively similar as the region over which adhesion occurs decreases dramatically as λ increases in magnitude whilst the value of σ_0 significantly increases. It is seen for $\lambda = 3$ that there are very large negative pressures which occur on the edges of the contact and correspond to high tensile stresses. This behaviour is similar to that predicted by the JKR model for a homogeneous solid. The curves produced for $\lambda = 0.3$ are qualitatively similar to those produced for the DMT model in the case of a homogeneous solid as the pressure curves observed here have a relatively small adhesive pressure and act over a wider area as compared to the results produced for larger values of λ.

The sub-surface stress fields (Tresca) produced using the pressure curves above are depicted in figure (13) and (14). We note that the change in λ has very little effect on the sub-surface stress field within the soft coating except immediately below the points $x = \pm c$ where an increase in λ and thus an increase in magnitude of the adhesive pressure yields a more pronounced principal stress. In fact, the sub-surface stress field produced for $\lambda = 3$ indicates that the stresses at the

points of pronounced adhesion are of the same order of magnitude as the maximum principal stress attained below the surface. Finally, we observe that the maximum dimensionless principal stress is approximately 0.25 which is less than the maximum stress predicted by Hertz (approximately 0.3) which indicates that material failure is less likely here.

The results presented in figure (14) which correspond to a hard coating indicate that the actual pattern of the sub-surface stress field is relatively unaffected by an increase in λ. However, we see here that the maximum principal stresses occur immediately below the surface where the adhesive pressures are applied and their magnitude is highly dependent on λ. The results presented for $\lambda = 0.3$ and $\lambda = 1$ indicate that the maximum dimensionless principal stress is similar to that predicted by Hertz whilst for $\lambda = 2$ and $\lambda = 3$ this value increases dramatically. These observations lead us to deduce that the high tensile stresses experienced on the surface at $x = \pm c$ will eventually cause hard coatings to fail and experience plastic flow for λ sufficiently large. This information could potentially be crucial in the design and manufacture of protective coatings.

8. Conclusions

Using the work of Chidlow et al. (2011a), we have formulated two non-singular integral equations of the first kind which utilise differing information to approximate the contact pressure applied on the surface of an inhomogeneous solid. The first integral equation assumes that the surface deflection is known over the contact region whilst the second integral equation is valid for contact by a rigid punch and assumes that the gradient of surface deflection is known within this region. As both integral equations are non-singular, their solution may be approximated using classical methods. The choice was made here to use Galerkin's method and thus the integral equations were

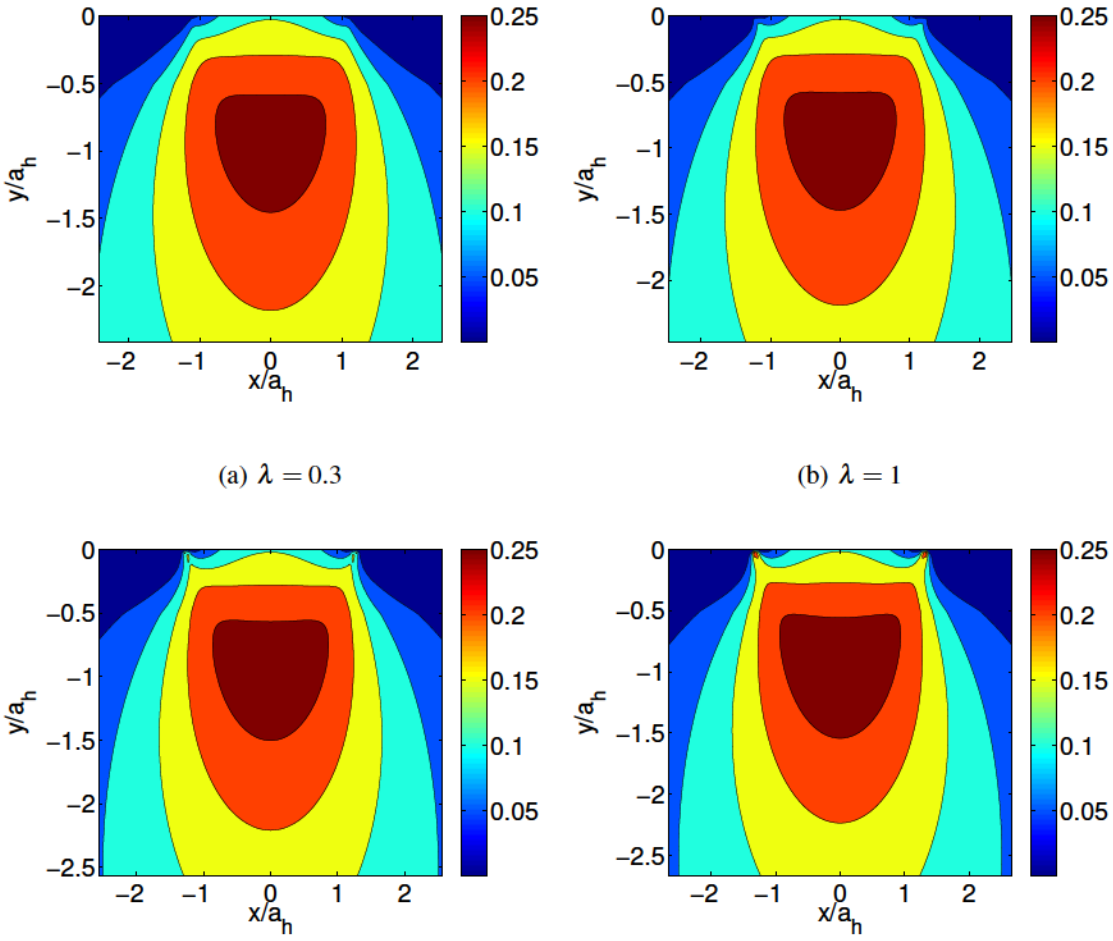

(a) $\lambda = 0.3$

(b) $\lambda = 1$

(c) $\lambda = 2$

(d) $\lambda = 3$

Figure 13: Contour plots of the principal stress field for the soft coating $\mu_1/\mu_0 = 0.5$ of thickness $h/a_h = 0.5$ subject to different values of the Tabor parameter.

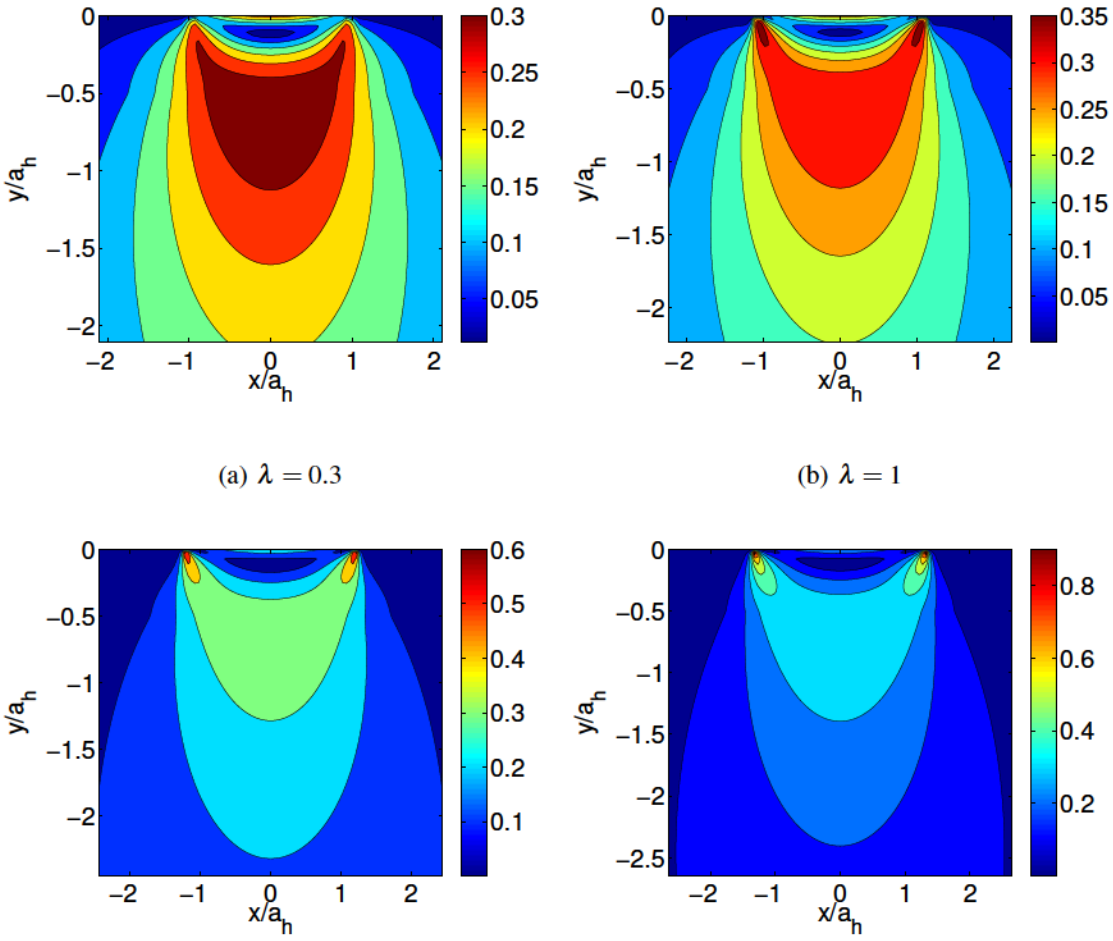

(a) $\lambda = 0.3$

(b) $\lambda = 1$

(c) $\lambda = 2$

(d) $\lambda = 3$

Figure 14: Contour plots of the principal stress field for the hard coating $\mu_1/\mu_0 = 2$ of thickness $h/a_h = 0.5$ subject to different values of the Tabor parameter.

replaced by a system of algebraic equations. The integral equation approximations were further extended by the derivation of an iterative algorithm based on the secant method used to simultaneously compute both the contact half-width and contact pressure.

A selection of numerical examples were presented to test the accuracy of the new approximations and it was found that the predicted results compare well with those of other authors. It was also found that whilst our results compare well with the Hertzian contact model in the limit $h/a_h \to 0$, our model begins to predict markedly different results as the ratio h/a_h increases. It was further noted that harder coatings tend to experience larger maximum principal stresses than softer coatings. These observations have been recorded by other authors (e.g. Teodorescu et al. (2009)) and provide a further check on the accuracy of this method.

This work concluded with a preliminary investigation into adhesive contact problems involving graded elastic solids. The assumptions of Maugis (1992) were invoked to include the effects of adhesion in the problem and an alternate integral equation was formulated to determine the pressure that results from adhesive contact. An iterative algorithm capable of determining both the contact half-width a and the new parameter c was proposed and used to produce numerical results for this problem. The so-called 'Tabor' parameter λ was used to characterise the adhesive energy in the problem and it was found that for $\lambda < 0.3$, the behaviour of the applied pressure is similar to that of the DMT model proposed for a homogeneous solid whilst for $\lambda > 3$ the pressure behaves in a similar way to that predicted by the JKR model. This indicates that whilst the quantitative predictions made by these models may not in general transfer to inhomogeneously elastic solids, the qualitative predictions remain accurate. These observations are very suggestive and indicate the

potential for further research in this area.

To summarise, the principal advantages of the solution techniques given in this work are

- the derived integral equations are non-singular and may be approximated using classical methods
- unlike the majority of alternate solution techniques, the total stress field may be easily computed at any point within the solid
- the underlying mathematical model is valid for graded elastic coatings which can be either hard or soft as well as thick and thin
- our model is capable of solving both adhesive and non-adhesive contact problems
- the proposed iterative scheme to determine the constants a and c are very simple in form and typically only a handful of iterations are needed to find both parameters to machine accuracy.

Appendix A. Contact model derivation

The following is a brief summary of how the contact model detailed in section 1 is obtained. For a fuller discussion, the reader is referred to Chidlow et al. (2011a).

It is found by seeking separable solutions of the displacements $u(x,y)$ and $v(x,y)$ in the coating that

$$u^{(c)}(x,y) = \sum_{n=1}^{\infty} \left(\sum_{j=1}^{4} a_j^{(n)} e^{\lambda_{j,n} y} \right) \cos\left(\frac{1}{2} \beta_n (x+L) \right), \qquad (-h \leq y \leq 0), \tag{A.1}$$

$$v^{(c)}(x,y) = -\sum_{n=1}^{\infty} \left(\sum_{j=1}^{4} \gamma_{j,n} a_j^{(n)} e^{\lambda_{j,n} y} \right) \sin\left(\frac{1}{2} \beta_n (x+L) \right), \qquad (-h, \leq y \leq 0) \tag{A.2}$$

where

$$\gamma_{j,n} = \frac{2\left((1-2\nu)\lambda_{j,n}^2 + \alpha(1-2\nu)\lambda_{j,n} - \frac{1}{2}(1-\nu)\beta_n^2\right)}{\beta_n\left(\lambda_{j,n} + \alpha(1-2\nu)\right)} \tag{A.3}$$

and the roots $\lambda_{j,n}$ satisfy the quartic equation

$$\lambda^4 + 2\alpha\lambda^3 + \left(\alpha^2 - \frac{1}{2}\beta_n^2\right)\lambda^2 - \frac{1}{2}\alpha\beta_n^2\lambda + \frac{\beta_n^2}{16}\left(\beta_n^2 + \frac{4\alpha^2\nu}{1-\nu}\right) = 0. \tag{A.4}$$

Explicit formulae for these roots give

$$\lambda_{1,n} = \sqrt{\frac{1}{4}(\alpha^2+\beta_n^2) + \frac{i}{2}\alpha\beta_n\sqrt{\frac{\nu}{1-\nu}}} - \frac{1}{2}\alpha, \tag{A.5}$$

$$\lambda_{2,n} = -\sqrt{\frac{1}{4}(\alpha^2+\beta_n^2) + \frac{i}{2}\alpha\beta_n\sqrt{\frac{\nu}{1-\nu}}} - \frac{1}{2}\alpha \tag{A.6}$$

$$\lambda_{3,n} = \sqrt{\frac{1}{4}(\alpha^2+\beta_n^2) - \frac{i}{2}\alpha\beta_n\sqrt{\frac{\nu}{1-\nu}}} - \frac{1}{2}\alpha, \tag{A.7}$$

$$\lambda_{4,n} = -\sqrt{\frac{1}{4}(\alpha^2+\beta_n^2) - \frac{i}{2}\alpha\beta_n\sqrt{\frac{\nu}{1-\nu}}} - \frac{1}{2}\alpha \tag{A.8}$$

and so $\lambda_{3,n} = \bar{\lambda}_{1,n}$, $\lambda_{4,n} = \bar{\lambda}_{2,n}$. The general solution of the displacements in the substrate are found to be

$$u^{(s)}(x,y) = \sum_{n=1}^{\infty}\left(C_1^{(n)} + C_2^{(n)}y\right)e^{\frac{1}{2}\beta_n y}\cos\left(\frac{1}{2}\beta_n(x+L)\right), \qquad (-\infty < y < -h), \tag{A.9}$$

$$v^{(s)}(x,y) = \sum_{n=1}^{\infty}\left(C_1^{(n)} + (y-\delta_n)C_2^{(n)}\right)e^{\frac{1}{2}\beta_n y}\sin\left(\frac{1}{2}\beta_n(x+L)\right). \qquad (-\infty < y < -h) \tag{A.10}$$

The constants δ_n are defined as

$$\delta_n = \frac{2(3-4\nu)}{\beta_n}. \tag{A.11}$$

Application of the matching conditions and surface boundary conditions given by (3c), (3d) and (3f)-(3i) give the constants appearing in the general solutions of the displacements above as

$$\begin{pmatrix} a_1^{(n)} \\ a_3^{(n)} \end{pmatrix} = W_n^{-1} \begin{pmatrix} \frac{(1-2\nu)}{2\mu_0} P_n \\ 0 \end{pmatrix}, \tag{A.12}$$

$$\begin{pmatrix} a_2^{(n)} \\ a_4^{(n)} \end{pmatrix} = -(T_{2,n}\mathscr{K}_{2,n})^{-1} T_{1,n}\mathscr{K}_{1,n} W_n^{-1} \begin{pmatrix} \frac{(1-2\nu)}{2\mu_0} P_n \\ 0 \end{pmatrix}, \tag{A.13}$$

$$\begin{pmatrix} C_1^{(n)} \\ C_2^{(n)} \end{pmatrix} = \frac{e^{\frac{1}{2}\beta_n h}}{\delta_n} \left(Z_{1,n} - Z_{2,n}(T_{2,n}\mathscr{K}_{2,n})^{-1} T_{1,n}\right) \mathscr{K}_{1,n} W_n^{-1} \begin{pmatrix} \frac{(1-2\nu)}{2\mu_0} P_n \\ 0 \end{pmatrix}. \tag{A.14}$$

The 2×2 matrices appearing in (A.12), (A.13) and (A.14) are defined as

$$W_n = N_{1,n} - N_{2,n}(T_{2,n}\mathscr{K}_{2,n})^{-1} T_{1,n}\mathscr{K}_{1,n}, \tag{A.15}$$

$$T_{j,n} = N_{j,n} + \frac{1}{\delta_n} M_{j,n}, \tag{A.16}$$

$$Z_{j,n} = \begin{pmatrix} \delta_n + h(1+\gamma_{j,n}) & \delta_n + h(1+\gamma_{j+2,n}) \\ 1+\gamma_{j,n} & 1+\gamma_{j+2,n} \end{pmatrix} \tag{A.17}$$

for $j = 1, 2$. The remaining matrices are

$$\mathscr{K}_{j,n} = \operatorname{diag}(e^{-\lambda_{j,n}h}, e^{-\lambda_{j+2,n}h}), \tag{A.18}$$

$$M_{j,n} = \begin{pmatrix} \frac{1}{2}(1-2\nu)\left(4(1-\nu)(1+\gamma_{j,n}) - \beta_n\delta_n\right) & \frac{1}{2}(1-2\nu)\left(4(1-\nu)(1+\gamma_{j+2,n}) - \beta_n\delta_n\right) \\ 2(1-2\nu)(1+\gamma_{j,n}) - \beta_n\delta_n & 2(1-2\nu)(1+\gamma_{j+2,n}) - \beta_n\delta_n \end{pmatrix} \tag{A.19}$$

$$N_{j,n} = \begin{pmatrix} -\left(\frac{1}{2}\nu\beta_n + (1-\nu)\lambda_{j,n}\gamma_{j,n}\right) & -\left(\frac{1}{2}\nu\beta_n + (1-\nu)\lambda_{j+2,n}\gamma_{j+2,n}\right) \\ \lambda_{j,n} - \frac{1}{2}\beta_n\gamma_{j,n} & \lambda_{j+2,n} - \frac{1}{2}\beta_n\gamma_{j+2,n} \end{pmatrix}, \tag{A.20}$$

$j = 1,2$. At this point we see that we may write the displacements in the coating as (5) and (6) with

$$\xi_n(y) = (e^{\lambda_{1,n}y}, e^{\lambda_{3,n}y}, e^{\lambda_{2,n}y}, e^{\lambda_{4,n}y})^T, \tag{A.21}$$

$$\Gamma_n = \mathrm{diag}(\gamma_{1,n}, \gamma_{3,n}, \gamma_{2,n}, \gamma_{4,n}), \tag{A.22}$$

$$\Omega_n = \begin{pmatrix} W_n^{-1} \\ -(T_{2,n}\mathscr{K}_{2,n})^{-1} T_{1,n}\mathscr{K}_{1,n}W_n^{-1} \end{pmatrix}. \tag{A.23}$$

The displacements in the substrate may similarly be written as (7) and (8). The previously undefined quantities appearing here are

$$\varphi(y) = (1,y)^T, \tag{A.24}$$

$$\Phi_n = \begin{pmatrix} 1 & -\delta_n \\ 0 & 1 \end{pmatrix}, \tag{A.25}$$

$$\Psi_n = \left(Z_{1,n} - Z_{2,n}T_{2,n}^{-1}T_{1,n}\right)\mathscr{K}_{1,n}W_n^{-1}. \tag{A.26}$$

Acknowledgement

The authors acknowledge the technical support from partners and sponsorship provided by the EPSRC through the ENCYCLOPAEDIC program grant

References

References

Barber, J.R., 1990. Contact problems for the thin elastic layer. Int. J. Mech. Sci. 31, 129–132.

Bradley, R.S., 1932. The cohesive force between solid surfaces and surface energy of solids. Phil. Mag. 13, 853–862.

Carpick, R.W., Ogletree, D.F., Salmeron, M., 1999. A general equation for fitting contact area and friction vs load measurements. J. Colloid Interface Sci. 211, 395–400.

Chidlow, S.J., Teodorescu, M., Vaughan, N.D., 2011a. Predicting the deflection and sub-surface stress field within two-dimensional inhomogeneously elastic bonded layered solids under pressure. Int. J. Solids Structures 48, 3243–3256.

Chidlow, S.J., Teodorescu, M., Vaughan, N.D., 2011b. A solution method for the sub-surface stresses and local deflection of a semi-infinite inhomogeneous elastic medium. Applied Mathematical Modelling , doi:10.1016/j.apm.2011.10.006.

Derjaguin, V., Muller, V.M., Toporov, Y.P., 1975. Effect of contact deformations on the adhesion of particles. J. Colloid Interface Sci 53, 314–326.

Fuller, K.N.G., Tabor, D., 1975. The effect of surface roughness on the adhesion of elastic solids. Proc. R. Soc. Lond. A. 345, 327–342.

Giannakopoulos, A.E., Suresh, S., 1997. Indentation of solids with gradients in elastic properties: Part 1. point force. Int. J. Solids Structures 34, 2357–2392.

Guler, M.A., Erdogan, F., 2004. Contact mechanics of graded coatings. Int. J. Solids Structures 41, 3865–3889.

Guler, M.A., Erdogan, F., 2007. The frictional sliding contact problems of rigid parabolic and cylindrical stamps on graded coatings. Int. J. Mech. Sciences 49, 161–182.

Hannah, M., 1951. Contact stress determination in a thin elastic layer. Q. J. Mech. Appl. Math. 4, 94–105.

Hertz, H., 1881. On the contact of elastic solids. J. Reine Angew. Math. 92, 156–157.

Johnson, K.L., 1985. Contact Mechanics. Cambridge University Press, Cambridge.

Johnson, K.L., Greenwood, J.A., 2008. A maugis analysis of adhesive line contact. J. Phys. D: Appl. Phys. 41, 155315.

Johnson, K.L., Kendall, K., Roberts, D.A., 1971. Surface energy and the contact of elastic solids. Proc. R. Soc. Lond. A. 324, 301–313.

Johnson, K.L., Sridhar, I., 2000. Adhesion between a spherical indenter and an elastic solid with a compliant elastic coating. J. Phys. D: Appl. Phys. 34, 683–689.

Ke, L.L., Wang, Y.S., 2006. Two-dimensional contact mechanics of functionally graded materials with arbitrary spatial variations of material properties. Int. J. Solids Structures 43, 5779–5798.

Ke, L.L., Wang, Y.S., 2007. Two-dimensional sliding frictional contact of functionally graded materials. European Journal of Mechanics A/Solids 26, 171–188.

Mary, P., Chateauminois, A., Fretigny, C., 2006. Contact deformation of elastic coatings in adhesive contacts with spherical probes. J. Phys. D: Appl. Phys. 39, 3665–3673.

Maugis, D., 1992. Adhesion of spheres: the jkr-dmt transition using a dugdale model. J. Colloid Interface Sci 150, 243–269.

McGuiggan, P.M., Wallace, J.S., Smith, D.T., Sridhar, I., Zheng, Z.W., Johnson, K.L., 2007. Contact mechanics of layered elastic materials: experiment and theory. J. Phys. D: Appl. Phys. 40, 5984–5994.

Porter, D., Stirling, D.S.G., 1990. Integral equations. Cambridge University Press, Cambridge.

Suli, E., Mayers, D.F., 2003. Numerical Analysis. Cambridge University Press, Cambridge.

Teodorescu, M., Rahnejat, H., Gohar, R., Dowson, D., 2009. Harmonic decomposition analysis of contact mechanics of bonded layered elastic solids. Applied Mathematical Modelling 33, 467–485.

Wu, J.J., 2009. Adhesive contact between a cylinder and a half-space. J. Phys. D: Appl. Phys. 42, 155302.